DESIGN OF FUNCTIONAL MATERIALS USING LIQUID CRYSTALS AS
MOLECULAR TEMPLATES

A THESIS SUBMITTED TO
THE GRADUATE SCHOOL OF NATURAL AND APPLIED SCIENCES
OF
MIDDLE EAST TECHNICAL UNIVERSITY

BY

ASLI KARAUSTA

IN PARTIAL FULFILLMENT OF THE REQUIREMENTS
FOR
THE DEGREE OF MASTER OF SCIENCE
IN
CHEMICAL ENGINEERING

SEPTEMBER 2018

Approval of the thesis:

DESIGN OF FUNCTIONAL MATERIALS USING LIQUID CRYSTALS AS MOLECULAR TEMPLATES

submitted by **ASLI KARAUSTA** in partial fulfillment of the requirements for the degree of **Master of Science in Chemical Engineering Department, Middle East Technical University** by,

Prof. Dr. Halil Kalıpçılar
Dean, Graduate School of **Natural and Applied Sciences** _____

Prof. Dr. Pınar Çalık
Head of Department, **Chemical Engineering** _____

Asst. Prof. Dr. Emre Büküşoğlu
Supervisor, **Chemical Engineering Dept., METU** _____

Prof. Dr. Halil Kalıpçılar
Co-Supervisor, **Chemical Engineering Dept., METU** _____

Examining Committee Members:

Prof. Dr. Levent Yılmaz
Chemical Engineering Dept., METU _____

Asst. Prof. Dr. Emre Büküşoğlu
Chemical Engineering Dept., METU _____

Prof. Dr. Halil Kalıpçılar
Chemical Engineering Dept., METU _____

Prof. Dr. Nihal Aydoğan
Chemical Engineering Dept., Hacettepe University _____

Assoc. Prof. Dr. P. Zeynep Çulfaz Emecen
Chemical Engineering Dept., METU _____

Date: _____

I hereby declare that all information in this document has been obtained and presented in accordance with academic rules and ethical conduct. I also declare that, as required by these rules and conduct, I have fully cited and referenced all material and results that are not original to this work.

Name, Last name : Aslı Karausta

Signature :

ABSTRACT

DESIGN OF FUNCTIONAL MATERIALS USING LIQUID CRYSTALS AS MOLECULAR TEMPLATES

Karausta, Aslı
MSc., Department of Chemical Engineering
Supervisor : Asst. Prof. Dr. Emre Büküşoğlu
Co-Supervisor: Prof. Dr. Halil Kalıpçılar

September 2018, 77 pages

Liquid crystal (LC) is a phase of material which is intermediate to a crystalline solid and an isotropic liquid such that the molecules flow but retain a degree of long-range orientational ordering. LCs, due to their long range orientational ordering and fluidic properties, can be used in templated synthesis of polymeric materials as well as self assembly of the microparticles incorporated into the LCs.

In the first part of this thesis, we sought to provide control over alignment of the polymer chains, alignment and size of the pores within polymeric films with thickness of 20-200 μm. For the synthesized polymeric materials, we used characterization methods such as thermal, optical, mechanical, nitrogen adsorption porosimetry and electron microscopy. As a result of these analysis, we found that it is possible to control both size distribution (between 5-50 nm-in-diameter) and alignment of pores, and the material exhibit alignment-dependent mechanical properties which are sufficient to be used in different applications such as separation, soft robotics, sensors and biomedical devices.

In the second part of the thesis, we investigated the self-assembly of the inorganic particles of different shapes incorporated into LCs. The zeolite 4A particles used were cubic particles with truncated, sharp or round edges in a size range of 2-6 μm. The ZIF-L particles used were leave shaped particles with 400 nm thickness and 1-4 and 5-10 μm in length and width, respectively. The particles were observed to orient in a

preferred direction and mediate anchoring conditions that lead to three-dimensional defect structures.

ÖZ

SIVI KRİSTALLERİN MOLEKÜLER ŞABLON OLARAK KULLANILMASIYLA FONKSİYONEL MALZEMELERİN TASARLANMASI

Karausta, Aslı
Yüksek Lisans, Kimya Mühendisliği Bölümü
Tez Yöneticisi:　　　Dr. Öğr. Üyesi Emre Büküşoğlu
Ortak Tez Yöneticisi: Prof. Dr. Halil Kalıpçılar

Eylül 2018, 77 sayfa

Sıvı kristaller, taşıdıkları akışkanlık ve bir dereceye kadar yönelim düzenlerini koruyabilme özellikleriyle aynı anda katı ve sıvı faz özelliği gösterebilen malzemelerdir. Bu özellikleriyle; polimerik malzemelerin tasarımları ve mikropartiküllerin organizasyonlarının kontrol edilebilmesi için şablon olarak kullanılabilmektedir.

Bu çalışmanın ilk bölümünde, kalınlığı 20 ile 200 mikrometre arasında değişen polimerik filmleri oluşturan polimer zincirinin ve içerdikleri gözeneklerin yöneliminin belirlenebilmesi ve gözenek boyutunun kontrol edilebilmesi üzerine çalışılmıştır. Sentezlenen malzemeler; ısıl, optik ve mekanik karakterizasyon metotlarının yanı sıra azot adsorpsiyonu ile gözenek ölçümü ve elektron mikroskobu ile görüntüleme yöntemleri kullanılarak karakterize edilmiştir. Bu analizlerin sonucunda, gözenek boyutunun (çap boyutu 5 ile 50 nm arasındadır) ve doğrultusunun kontrol altına alınabileceği ve yönelime bağlı mekanik özellik gösteren, ayırma işlemleri, sensör uygulamaları ve biyomedikal cihazlar gibi farklı uygulamalarda yer alabilecek bir malzemenin sentezinin mümkün olduğu gösterilmiştir.

Çalışmanın ikinci bölümündeyse, farklı şekillerdeki inorganik mikroparçacıkların sıvı kristal ortamda oluşturdukları yapılar incelenmiştir. Bu analizlerde yuvarlatılmış kenarlı, kesik kenarlı ve keskin kenarlı, boyutları 2 ile 6 mikrometre arasında değişen küp şeklindeki zeolite 4A parçacıkları kullanılmıştır. Ayrıca yaprak şeklindeki 400 nm kalınlığında, uzunluğu 5 ile 10 μm, genişliği 1 ile 4 μm arasında değişen ZIF-L parçacıkları kullanılmıştır. Çalışmaların sonunda, parçacıkların yöneliminin istenen

doğrultuda sağlanılabildiği ve sıvı kristalin tutunma koşulları değiştirildiğinde üç boyutlu kusur yapılarının oluştuğu görülmüştür.

Anahtar Kelimeler: Sıvı kristal, şablon sentez, polimerizasyon, mezo-gözenekli filmler, ultrafiltrasyon

To my family

ACKNOWLEDGMENTS

TABLE OF CONTENTS

APPENDICES

LIST OF TABLES

TABLES

LIST OF FIGURES

FIGURES

non-reactive mesogen 4-cyano-4′-pentylbiphenyl (5CB) used in this study. (b) Schematic illustration of the experimental procedure showing polymerization of RM257 and extraction of 5CB. (c) Photograph of an 80 μm-thick polymeric film synthesized from 20% wt RM257 and 80% wt 5CB with planar anchoring. Scale bar: 1 cm (d) Bright field (left) and polarized (middle and right) light micrographs of the polymeric films (20% RM257) with planar (top row) and homeotropic (bottom row) anchoring. Inset showing conoscopic image of the film. Scale bars: 50 μm 24

CHAPTER 1

INTRODUCTION

Design of chemical processes such as separation systems or reaction systems rely mostly on the mass transfer rates of the substances involved in these processes. If there are any limitations of the mass transfer rates, the performances of the chemical processes are also limited. In the end, these poor conditions may result in unfeasible designs of the processes. The alignment and size scale of the media that the chemical species are present, however, have been shown to play an important role on improving the mass transfer rates of the species[1]. If a control over the alignment and size scale of the materials can be achieved, the design of the chemical processes can also be easily improved. One practical option to provide nano- and mesoscale alignment to the materials is the use of liquid crystals as templates during their synthesis.[2–4]

Liquid crystals (LCs) are phase of matter intermediate to a crystalline solid and an isotropic liquid. They exhibit long range orientational ordering (up to 100 μm in length) similar to the crystals and they flow when stress is applied similar to the fluids. LCs are classified into two groups which are thermotropic and lyotropic liquid crystals.

The phase behavior of the thermotropic liquid crystals (TLCs) is changed by temperature as represented in Figure 1.1. As the temperature increases, TLCs start to lose their long range orientational order but gain high mobility and melt to their isotropic phases.[2] Nematic phases of thermotropic LCs possess orientational ordering towards a uniform direction called *director* but exhibit no long-range positional order. When mixed with chiral dopants (Figure 1.1f for example), cholesteric liquid crystals can form. Cholesteric liquid crystals are characterized by a periodic helical twist that is orthogonal to the nematic director of the constitutive mesogens. They are characterized by a pitch size, the length at which a twist of 2π occurs, which is a function of the concentration of the chiral dopants (see Figure 1.1e as an example chiral dopant molecule). The pitch size of the cholesteric liquid crystals can be in the order of 100 nm, which may give rise to reflections of light at visible wavelengths.[5]
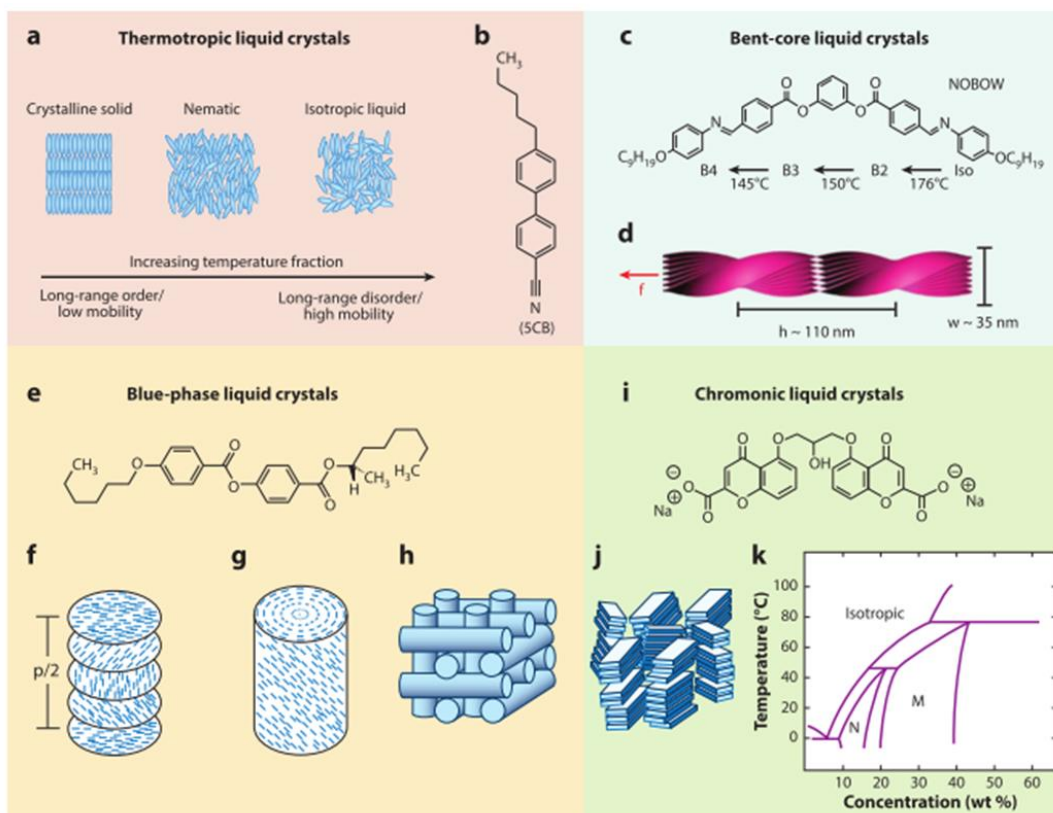
Figure 1.1 (a) Schematic illustration of (a) the phase behavior of thermotropic LCs and (b) molecular structure of pentyl cyanobiphenyl (5CB) which is a non-reactive mesogen used in this study, (c) an example for a bent core liquid crystal (d) a sketch that represent bent core liquid crystal ordering symmetry (e) Molecular structure of chiral dopant (S-811) (f) schematic representation of the structure of cholesteric phase (g) double twist structure and (h) blue phases of the liquid crystals. (c) an example for a lyotropic liquid crystal disodium cromoglycate (DSCG) (d) a sketch that represent chromonic lyotropic ordering symmetry, and (k) phase behavior of DSCG that is an example of lyotropic LC formed by dispersing polyaromatic, nonamphiphilic molecules in a solvent (called as chromonic)[2]

Lyotropic liquid crystals exhibit liquid crystalline phases as a function of temperature and chemical composition of the material. Lyotropic liquid crystals are usually formed by the dissolution of amphiphilic molecules in solvents. An example phase diagram of a common chemical disodiumchromoglycate (DSCG) in water is shown in Figure 1.1k.

When using liquid crystals in the design of materials, there are three key concepts that require special attention. These concepts can be summarized as surface anchoring, elasticity and the formation of topological defects. Below, explanations of these three concepts are summarized.

(A) Surface anchoring

n_s (surface director)

n_e (easy axis)

n

interface

$$F_S = F_0 + \frac{1}{2}W_a(\theta_s\text{-}\theta_e)$$

$W_a \sim 10^{-3}\text{-}10^{-2}\,mJ/m^2$

(B) Elasticity of liquid crystals

$$F_{el} = \frac{1}{2}K_1(\nabla \bullet \underline{n})^2 + \frac{1}{2}K_2(\underline{n} \bullet \nabla \times \underline{n})^2 + \frac{1}{2}K_3(\underline{n} \times (\nabla \times \underline{n}))^2$$

Splay   Twist   Bend

$K_i \sim 10^{-11}\,N$

$L \sim K_i/W_a \sim 1\text{-}10\ \mu m$

(C) Topological defects

$$F_d = \int_{V_d} f_d\, dV_d \sim \frac{4}{3}\pi r_d^3\, \epsilon_d$$

$$r_d \sim \sqrt{\frac{K}{\varepsilon_d}} \sim 5\ nm$$
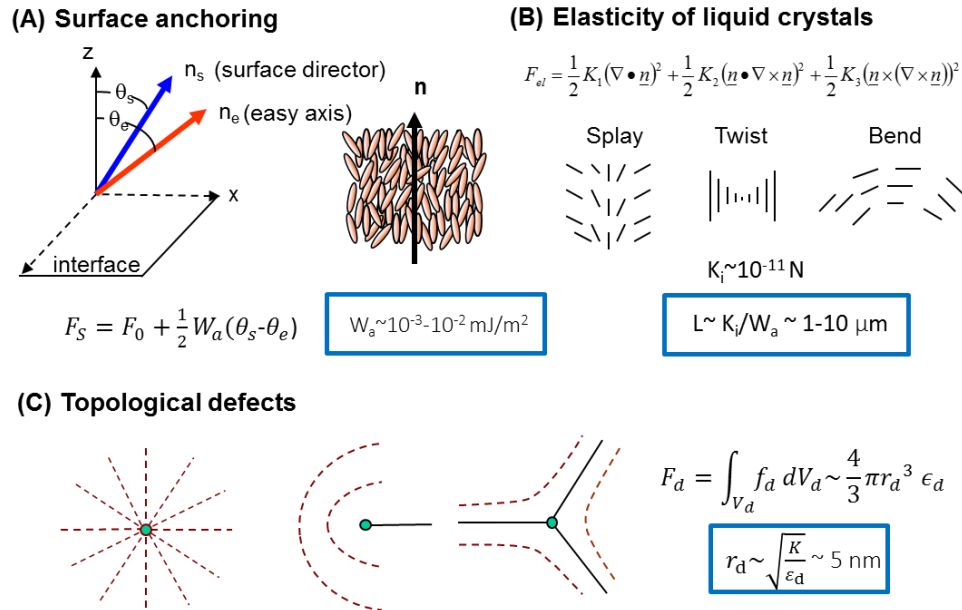
Figure 1.2 Schematic illustrations of (a) the director and easy axis of a liquid crystal (LC) anchored at a surface and expression for F_s, anchoring energy; (b)the three basic modes of deformation of a LC (splay, twist, and bend) and an expression for F_{el}, the elastic free energy density, that results from these strains; and (c) three types of topological defects that can form in a LC: (left) a point defect located at the center of a radially converging director field, and (center, right) cross-sections of line defects (disclinations). The line defects are oriented orthogonal to the plane containing the figure and F_d, represents the energy of formation of a defect.[2]

The surface anchoring results from the intermolecular interactions between the LCs and their contacting interfaces. In the absence of external fields, the lowest free energy orientation of the LC director is defined as the easy axis (Figure 1.2a). When an external field (magnetic field, light, heat etc.) is applied, the director starts to deviate from the easy axis (Figure 1.2a), which penalized by an energy that is a function of the

anchoring energy, W (J/m^2), and the extent of the deviation from the easy axis.[2] If the molecules are aligned perpendicular to the surface, the anchoring is called homeotropic anchoring (Figure 1.3a). If the alignment of the molecules is parallel to the surface, then it is called planar anchoring (Figure 1.3b). If the azimuthal anchoring is fixed, the LC molecules exhibit a uniform planar anchoring at the surfaces. If not, their anchoring is degenerate. It is possible to predetermine the anchoring of the LCs by functionalizing the surfaces in contact with liquid crystals. For example, rubbed polyvinylalcohol (PVA) surfaces are used for uniform planar anchoring, whereas, octyltrichlorosilane (OTS) functionalized surfaces are used for homeotropic anchoring of the nematic phases of 5CB or E7.
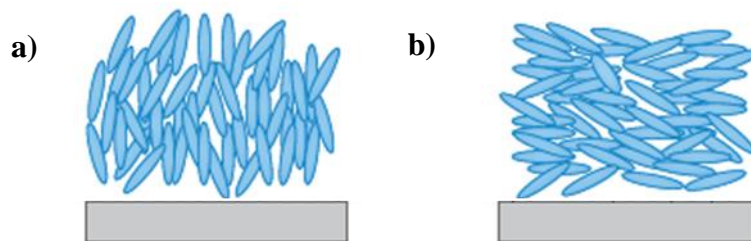
Figure 1.3 Schematic representation of (a) homeotropic anchoring and (b) planar anchoring

Another key concept is the elasticity of liquid crystals that provides the long range orientational ordering. When in contact with a surface in a confined environment, LCs may be strained in order to meet the boundary conditions (surface anchoring) set by the confined system. There are three fundamental modes of straining LC ordering in the simplest cases. These are twist, bend and splay (Figure 1.2b). When the elastic energy associated to a strain (~KL, K is the elastic constant of the LCs, ~10^{-11} N, L is the size scale of the confined system) and anchoring energy associated to an LC and a surface (~WL^2, W is the anchoring energy, ~10^{-5} -10^{-6} J/m^2) are compared, it shows that a length between 1 to 10 micrometers determines whether the surface anchoring or the elasticity dominates the ordering of LCs. Below this range, elasticity dominates whereas above this range, anchoring energy dominates the ordering of the LCs and this situation poses another key concept that is topological defects (Figure 1.2c).

Topological defects, which are singularities in the LC ordering profile, form in LCs when internal constraints or external boundary conditions cannot be satisfied by continuous strain of the LC director. Typical value for radius of the defect cores is approximately 5 nm and it is possible to have control over the type of the topological defects such that they can be as point or ring shaped.

Successful application of these three key concepts, LCs can be aligned in predetermined configurations within confined systems. In order to use these configurations in the synthesis of aligned, structured polymeric materials, mesogenic molecules with reactive groups have been used extensively.[6] Reactive mesogens usually consist of a mesogenic core with considerable rigidity, and reactive groups such as acrylate or epoxy functionalities. These reactive groups can be present at the two ends, at a single end or at the side of the mesogenic core (Figure 1.4). The choice of the reactive mesogen type depends on the intended application of the final material to be synthesized.[7–11] When mixed with non-reactive LCs or present at their LC phase conditions, alignment can be given to these molecules. With the presence of a photoinitiator, these molecules can easily be crosslinked to form structured polymeric materials.
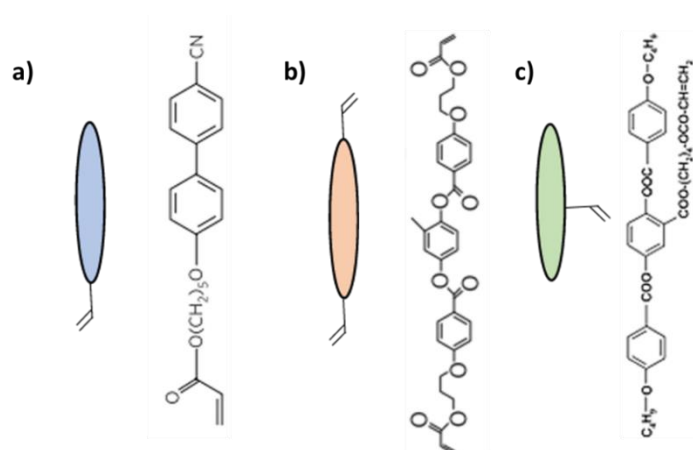
Figure 1.4 Schematic illustrations and the molecular structures of reactive mesogens that the reactive group located at (a) single end (RM23), (b) two ends (RM257) and (c) side of the mesogenic core (4-ADBB)

In addition to the polymeric materials with specified internal structure, materials composed of nanometer/micrometer sized particles organized by regular structures exhibit many advantageous optical, mechanical and catalytical properties.[12–16] Therefore, beside determination of the internal structure of the polymeric materials at molecular level, providing a control over the organization of the colloids with micrometer size in polymeric matrix by using the liquid crystal as templates is also desired. Guided by the above three concepts, the organizations of the microparticles in LC media is dependent on the shape, size and anchoring conditions of the LCs at the surfaces of the incorporated microparticles as they relate to the elasticity, surface anchoring and defect structures formed in LCs.

In this study, methods for the synthesis of polymeric materials with complex internal structures and organized colloidal assemblies were developed. Specifically, polymeric films (with and without microparticles) were synthesized using non-reactive liquid crystals to template the polymers that were obtained from photopolymerization of the reactive mesogens. The characterizations of the nanostructure, porosity, optical properties, thermal properties, and mechanical properties were done on the synthesized films. Finally, the mass transfer properties of the films were investigated. The methods and materials reported herein may find use in a range of applications including separations, soft robotics, sensors and biomedical devices.

CHAPTER 2

LITERATURE SURVEY

To date, there have been different successful studies about the synthesis methods involved the liquid crystals that provide advanced optical properties (anisotropy)[17,18], mechanical properties[9,19–26]and responsive properties (upon heating, exposure to light or chemicals)[27–29] to be able to broaden the application area of the polymeric materials. Therefore, today the polymeric materials templated from the liquid crystal can be used in several applications. Examples of such polymers include self-cleaning surfaces with oscillating surface topology upon an external electric field[30], liquid-release media that responds upon exposure to light[31], light-driven actuators[19,20,32–34], molecular motors[21,33] and artificial cilia[10]. These examples clearly demonstrated that the bulk response of the LCs could be obtained which originated from externally-triggered molecular-scale events occurring within the anisotropic media.

Polymer dispersed liquid crystals (PDLC), polymer stabilized liquid crystals and elastomers are the materials synthesized with the mainly preferred methods that involve the self-organization of the liquid crystals into polymeric network. In these methods, polymerization was performed by using the monomers and non-reactive liquid crystals, so it was possible to provide control over the response of the material when an external field was applied.[17,35–38] The monomers in these studies are not only non-mesogenic reactive monomers[39,40], but also monofunctional and difunctional mesogenic monomers that have been used to synthesize responsive polymeric materials in different forms of elastomers like droplets and films.[7,19,41–47]

PDLCs are the composite materials that a polymer network involve small amount of liquid crystals. They are generally synthesized by using the mixture of LC and non-mesogenic monomers and LC-rich and polymer-rich phases are formed within the polymeric network through demixing during polymerization. The morphology of the LC-rich domains is observed to be of usually disconnected, spherical domains within polymer-rich network with the size of microns.[39,48–50]

As it can be seen in Figure 2.1, micron-sized LC droplets are randomly embedded in a continuous polymer matrix. Therefore, it can be said that this method is not sufficient for this study since it can provide neither a specified alignment for the polymer chains nor aligned and accessible pores into the polymeric structure.
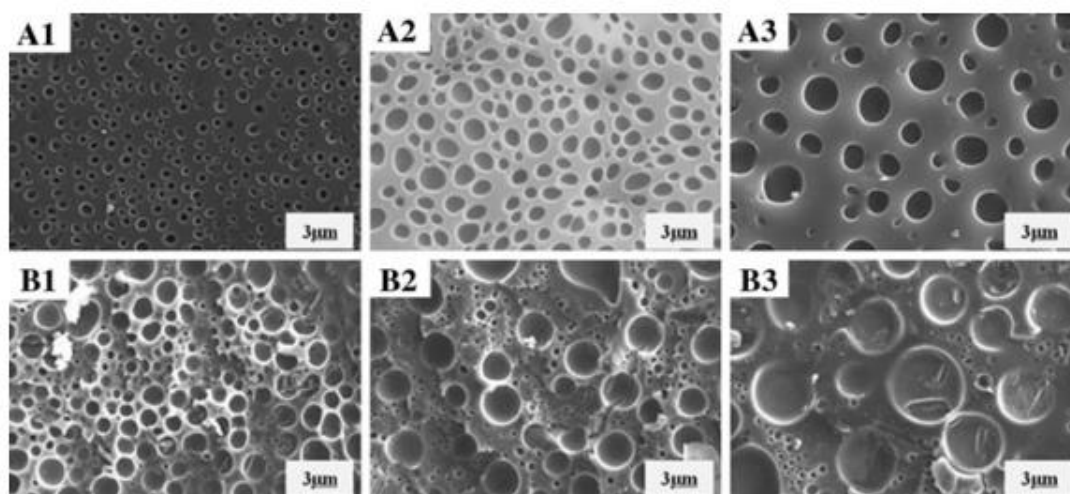
Figure 2.1 Scanning electron microscopy micrographs of the samples synthesized with different curing temperature

Liquid crystalline elastomers (LCEs) behave like both the polymeric elastomers and liquid crystals by combining their properties of entropy elasticity and self-organization. They are synthesized by using monoacrylate and diacrylate mesogens. The molecular structures of LCEs contain the long chains that are formed by the molecules, which are able to move one from another easily, so they make the material capable to expand against even very little force. Therefore, these materials can be synthesized to use as actuators and sensors by controlling their response to external stimuli such as heat, light, humidity etc. (Figure 2.2).[7,19,22,29,41–43,51–55] In order to provide response of different external stimuli, different procedures are applied for the synthesis. For the synthesis of photosensitive materials, LC molecules that contain photoisomerizable groups such as azobenzene are used.[20,21,24] In order to make the material responsive to humidity, bilayer polymers are synthesized by using substrates such as polyamide6 (PA-6).[27] In addition, by converting the hydrogen bonds in

reactive mesogen mixture to carboxylic salt, it is possible to provide a response to material to change in pH[8].
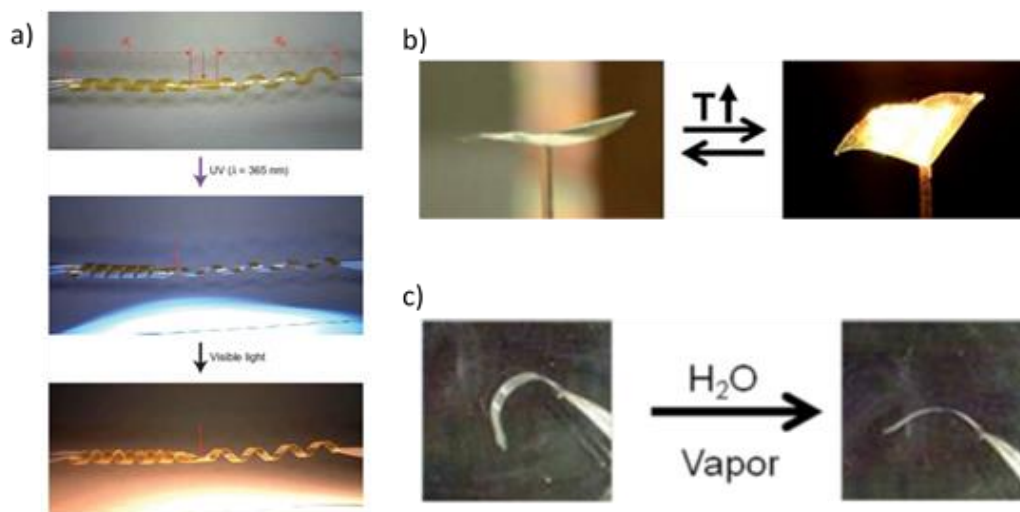
Figure 2.2 Examples of the polymer that are responsive to a) UV light b) heating c) humidity [27,46]

There are studies that involved the lyotropic liquid crystals (hexagonal, lamellar, columnar or cubic phase) or thermotropic smectic phases (due their layered structure) was employed as templates during the synthesis.[56–62] In these studies, nanoporous polymeric materials were synthesized and used with porous supports in membrane applications for gas and liquid separation processes (Figure 2.3) but control over the microstructure of the material was limited since these LC phases require certain conditions and chemicals to form and the synthesis methods were limited to those conditions.
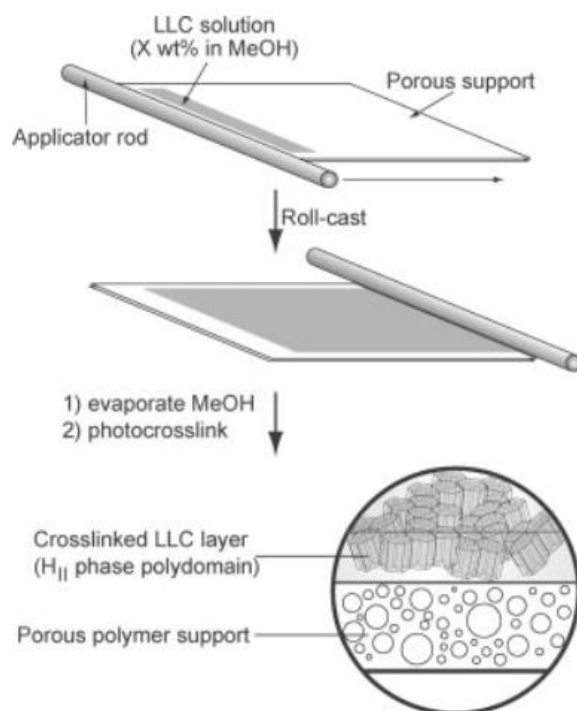
Figure 2.3 Schematic illustration of the procedure for the preparation of supported LLC membrane on porous polymer support (polysulfone) with solution-casting method

The mixture of the reactive (monoacrylate and diacrylate) and non-reactive mesogens were also used to synthesize the materials in different forms like polymeric films and droplets. For example in previous studies, the mixtures of reactive and non-reactive mesogens were polymerized in the forms of droplets that were produced in aqueous emulsions.[3,63,4,64–66] In these studies, LC droplets were synthesized with bipolar, radial, axial and preradial configurations.(Figure 2.4) They were polymerized and the unreacted part was extracted. Then, the internal structures of polymeric microparticles were characterized. When these particles were extracted and non-reactive mesogens were separated from the polymer, anisotropic shrinkage occurred, so the shapes of the particles were varied with respect to the initial droplet configurations. Therefore, LC droplets maintained different shapes such as spindle, spherical, tear drop and spherocylindrical shapes dependent on the initial configuration of the droplets. Furthermore, the mesoscale porosity was evident in the microparticles that were

10

synthesized from LC droplets with radial configuration that did not exhibit substantial shrinkage upon extraction of the non-reactive mesogens.[3,63] The reason of this non-shrinking behavior was considered to be due to the symmetry of the radial configuration that did not allow a major shrinkage of the microparticles upon extraction. Besides these, studies involving polymerization of LC shells demonstrated similar morphologies.[52] Therefore, these studies have showed that it is possible to provide control over the final shape, nano- and mesoscale structure of the microparticles using LCs as templates.
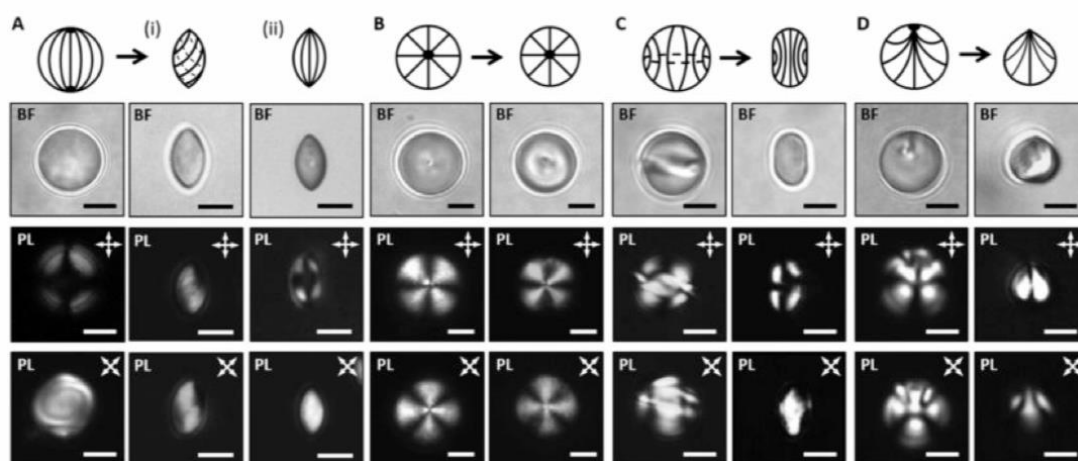
Figure 2.4 Synthesis of A) spindle-shaped, B) spherical, C) spherocylindrical or D) tear-shaped polymeric microparticles templated from LC droplets in (A) bipolar, (B) radial, (C) axial or (D) preradial configurations, respectively. The left and right columns for each shape show schematic illustrations and the corresponding bright field (BF) and polarized light (PL) images of polymerized LC droplets before and after extraction of 5CB, respectively. The orientation of the crossed polarizers in the PL images is indicated by the white double-headed arrows. We note that the disclination line is distorted in the images of the axial droplets shown in (C). Scale bars: 5 µm.

Overall, synthesis methods that were described to date were usually based on certain geometries or certain types of LCs. Thus, there is a need of a more generalizable and scalable synthesis methods that allow control over the ordering and porosity at the nano and meso scale.

11

In addition, recent studies aimed to improve the gas separation properties of polymers have focused on controlling the diffusion properties of the penetrant through various chemical and thermal applications or controlling the solubility properties by changing the polymer structure.[67–69] Paul and Kemp have shown that when they placed inorganic microparticles (zeolite-5) to the pure polymer structure, the hybrid material that they have obtained has a longer diffusion time than the pure polymer.[70] Also, Leddy and colleagues showed that the rate of gas diffusion is about two times faster in the direction of polymer orientation than in other directions.[1] However, it has not yet been found in the literature that this property created by the polymer orientation is used in the composite membranes and the contact of the inorganic particles with the gas molecules is increased. For this purposes, liquid crystal templated synthesis of microparticle doped polymeric materials with specified internal structure was also investigated in this study. Therefore, the parameters which have significant effect on the orientation of colloids in liquid crystal have an important role in this study.

The following examples from the literature demonstrate the effects of the parameters which are anchoring condition on the surface of the particle, size and shape of the particle, on three abovementioned concepts (surface anchoring, elasticity of liquid crystals and topological defects).

The effects of the alignment of the liquid crystals with different directions that contact with the surface of the particles on the organization of the particles were investigated by using spherical particles (Figure 2.5).[71,72] For example, Poulin and Weitz demonstrated that the chain of the particles, which have tangential anchoring on their surface, aligns at an angle of 30° from the far-field director (Figure 2.5d).[72] Also, Musevic and his collaborators functionalized the surface of the particles with diameter of 2.32 μm and provided the homeotropic anchoring of the liquid crystal (Figure 2.5b, c). As a result they could adjust the forms of defects occurred around the particle as satellite point or Saturn ring. They also demonstrated that the particles with satellite point defect form multiple orientation as straight chain whereas the particles with Saturn ring defect construct the assemblies as kinked chains (Figure 2.5e-g). These different forms of the organizations of the particles and the chains of them can be explained by the minimization of the energy penalties that occur because of the defects caused by the deviation of the liquid crystal alignment on the surface of the particles.
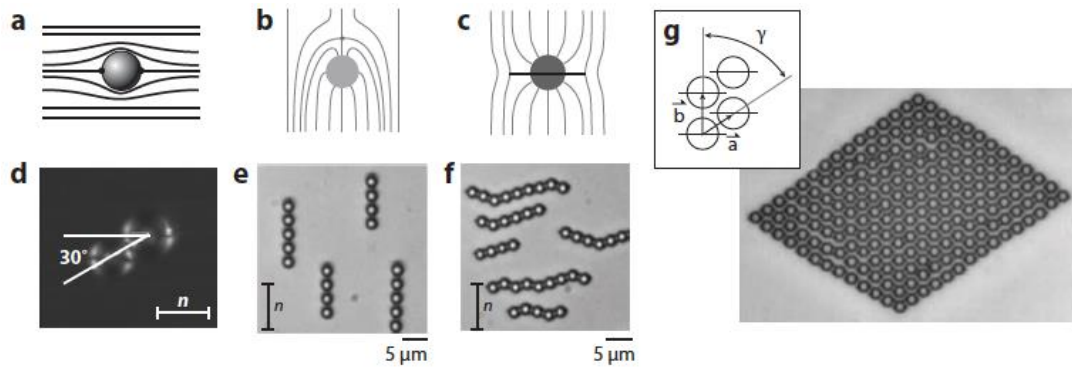
Figure 2.5 Structures of the defects and organizations of the spherical particles that exhibit different liquid crystal alignment in nematic liquid crystalline media. Schematic representation of the alignment of the liquid crystal around (a) tangential anchoring, (b,c) homeotropic anchoring (point and line represent the satellite point and Saturn ring, respectively), (d) Assembly of two particle which have tangential anchoring, (e, f) Chains of the particles with satellite point and Saturn ring. (g)Two-dimensional colloidal crystal formed by particles with Saturn ring defects. *n* indicates the nematic director.

Another parameter which affects the alignment of the liquid crystal in the vicinity of the particle and the structure of defects is the size of the particle. Loudet and his collaborators demonstrated that spherical particles in small size with homeotropic anchoring have very little effect on the orientation of the liquid crystal around them, thus they also indicated that the multiple organizations of the particles are randomly located in the liquid crystals (Figure 2.6a,c).[73] However, larger particles with the same composition align in the same direction of the liquid crystal alignment because of the satellite point defects (Figure 2.6b,d).[73] The range where the size of the particle has the importance is the proportion of the surface anchoring energy (~WR^2, W surface anchoring energy of unit area, ~10^{-5} - 10^{-6} J/m^2) to elastic energy (~KR, K elastic constant, ~10^{-11} N), basically. Therefore, it can be said that the critical size of the particles is in the range of 1- 10 μm. In general, the particles with the size below this range have little effects on the organization of the liquid crystal whereas the particles with the size above this range have significant effect on the liquid crystal alignment.

Therefore, for determination of the organization of the particles, the size of the particles is the critical parameter.
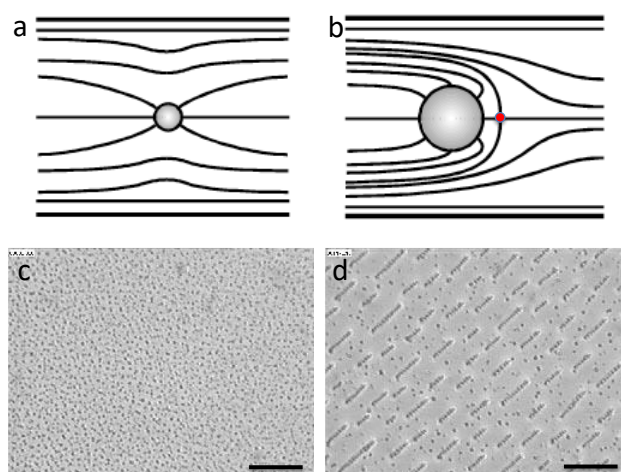
Figure 2.6 The liquid crystal orientations around the silicone oil droplets in various sizes and the distribution of the droplets in the liquid crystal medium. The schematic representation of the distortions around (a) small particles and (b) large particles (red point indicates the satellite point defect.) (c) the randomly located chains of small (< 2 μm) droplets and (d) the chains of the large (> 2 μm) droplets that align in the direction of nematic director. Scale bars: 60 μm.

The effect of particle shape on particle organization in liquid crystals has not yet fully been studied in the literature. Recently, the experimental studies of Lapointe and his collaborators and the simulation studies of Hung and Bale demonstrated that the interaction of the particles that have different shapes (cube, triangle and pentagonal prism) is strongly related to the orientation of these particles towards each other (Figure 2.7).[74,75] This effect varies depending on the orientation of the particles with respect to the general liquid crystal orientation and the strain of the liquid crystal in the vicinity of the particle. As a result, the organization of the particle is the liquid crystalline media is strongly affected. Lapointe and his collaborators also showed in their study that these particle can form perfect assemblies as the multiple (double and triple) organizations but the organization of the particles in higher concentrations and the effects of the size and the surface anchoring of the particles have not been studied

14

yet (Figure 2.7d-f).[74] In addition, how the particles that have different shapes in one and two dimensions such as rods, leaves, etc. will take place in liquid crystals and what kind of assemblies they will form in multiple organizations have not yet been investigated. The different particle shapes will affect the interaction between the particles and play a critical role in the multiple organizations.
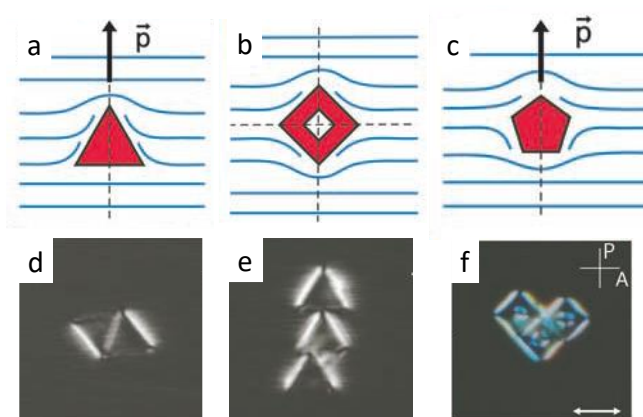
Figure 2.7 Schematic representation of the distortions of nematic liquid crystal around the particle with planar anchoring with the shape of (a) triangular prism, (b) cube and (c) pentagonal prism. Images of particles with the shape of (d, e) triangular prism and (f) cube in liquid crystal under polarized light microscope (Double headed arrow and crossed line indicate the nematic director and the direction of the polarization of the polarizer and analyzer, respectively).

Synthetic inorganic particles (zeolites, metallic organic frames (MOFs), etc.) can be synthesized with different shape as shown in Figure 2.8.[76–80] It is possible to synthesize the particle with the size in range of 10 nm-10 μm and due to their porous structures in molecular scale they can act as molecular sieves. Therefore, in both the literature and industry, they can be typically used in different processes like adsorption, gas and liquid separation, etc.[81–83] These applications and studies generally contain pure zeolite layers, metallic organic frame layers or composite membranes that involve randomly dispersed particles in conventional polymer.[81,82] Pure inorganic membranes are rarely preferred due to the difficulties in conditions of use and also the cost of the

applications. Also, polymer-inorganic composite membranes have disadvantages such as particle-polymer incompatibility and difficulty in finding sufficient solvent.[84,85]
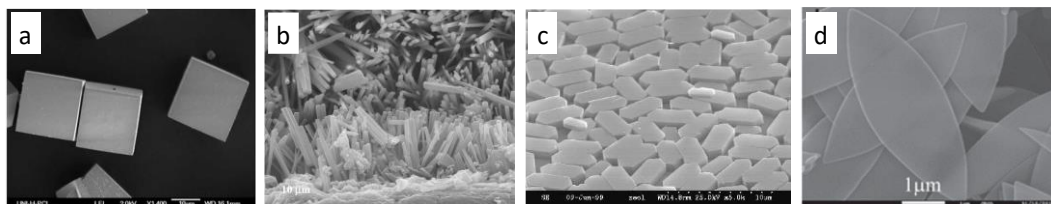
Figure 2.8 Examples of the several inorganic zeolite and metal organic frame particles. Scanning electron micrographs of (a) zeolite 4A, (b) mordenite, (c) ZSM-5 and (d) ZIF-L

Recent studies in the literature enable to adjust the alignment of the liquid crystal by functionalization of the surface of the inorganic materials. It is possible to vary the alignment of the liquid crystal as homeotropic or tangential by covalent attachment or physical attachment of chemicals like small molecules containing silane or thiol group or the polymers to particle surfaces and it also provides controlling the structure of the defects.[12,72,86,87] Therefore, surface functionalization methods are also important techniques for controlling the liquid crystal alignment and the forms of the defects.

In consideration of all the results of these previous studies, the objective of this study is to design a method for the synthesis of mesoporous polymeric films that go beyond the currently available examples by providing a facile, scalable and a universal tool that can be employed to a wide range of LC phases. By using this method, it can be possible to provide control over the alignment of polymer chain, size and direction of the pores and also the organization of the microparticles in polymer.

CHAPTER 3

MATERIALS AND METHODS

3.1. Materials

4-cyano-4′-pentylbiphenyl (5CB), E7 and 4-(3-acryloyoxy-propyloxy) benzoic acid 2-methyl-1,4-phenylene ester (RM257) were purchased from HCCH Jiangsu Hecheng Chemical Materials Co., Ltd. Polyvinyl alcohol (PVA), 3-(trichlorosilyl)propyl methacrylate, dimethyloctadecyl[3-(trimethoxysilyl)propyl]ammonium chloride (DMOAP), photoinitiator (1-hydroxycyclohexyl phenyl ketone), anhydrous methanol, anhydrous acetone and toluene were obtained from Sigma-Aldrich. Anhydrous ethanol was purchased from J.T. Baker. Perfluorodecyltrichlorosilane (PFDTS) was purchased from Alfa Aesar. 3-(trichlorosilyl)propyl methacrylate (TCSPM) was purchased from TCI Chemicals (Japan). Sulfate-coated 200 nm-in-diameter polystyrene particles were obtained from Life Technologies. 4-(1-methylheptyloxycarbonyl)phenyl-4-hexyloxybenzoate) (S-811) was purchased from Merck. Glass slides were obtained from Marienfeld (Germany). Sharp edged zeolite4A, truncated edged zeolite 4A and ZIF-L were donated from Salih Kaan Kirdeciler, Berna Topuz and Halil Kalıpçılar, respectively.

3.2. Preparation of Liquid Crystal-Monomer Mixtures

For the mixtures of liquid crystal and monomer, non-reactive mesogen 5CB and the reactive LC monomer RM257 was added at 10%-40% wt/wt. Also, the photoinitiator 1-hydroxylcyclohexyl phenyl ketone was added at 5% wt/wt based on the mass of RM257 to the mixture. For chiral LC mixtures, S-811 was added as chiral dopant and a liquid crystal mixture, E7, was used due to its higher nematic-isotropic phase transition. In order to solve the liquid crystal and prepare a homogenous solution, toluene was added as a solvent and mixed using vortex mixer until a clear solution was obtained. Then, toluene was evaporated from the solution under vacuum.

3.3. Preparation of Liquid Crystal-Microparticle Mixtures

In order to disperse the particles, they were put into solvent with a concentration of approximately 1g/L. For sharp and truncated edged zeolite4A, ethanol was used as solvent. For ZIF-L methanol was preferred since ethanol changes the structure of the particles. The particles were dispersed in the solvent by using vortex mixer and ultrasonic bath for 10 minutes. ZIF-L was not put into ultrasonic bath since it damages the particles, so dispersion of the particles was provided by only using the vortex mixer. Then, 30 µl of particles in solvent were taken and put into vial for 100 µl 5CB and mixed by using vortex mixer until the solution became clear. Then, in order to evaporate the solvent, the vial was stayed under vacuum for approximately 4 hours. For the mixture of the liquid crystal and monomer with the microparticles, the particles in solvent were taken and put into vial and the vial was placed in vacuum to evaporate the solvents. Therefore, it was provided that dispersed and dried particles were kept in vial. Then, the mixture of liquid crystal, monomer and photoiniator was prepared in this vial in the same way that explained above.

3.4. Cleaning of the Glass Surfaces

Before functionalization of the glass surfaces by DMOAP, PFDTS, or TCSPM, O_2 plasma was applied to the glass slides using a Diener Electronics, Zepto Plasma Unit. O_2 was fed to the system with a flow rate of 100 cm^3/min for 15 minutes for the plasma cleaning.

3.5. Functionalization of the Glass Surfaces

The surfaces of the glass slides and cover slips were functionalized with different chemicals. Polyvinyl alcohol (PVA) was used for the planar anchoring. The surfaces were coated by the spin coater (5000 rpm for 2 minutes) with 5% wt PVA in water solution using a Polos Spin Coater System. Perfluorodecyltrichlorosilane (PFDTS), Dimethyloctadecyl[3-(trimethoxysilyl)propyl]ammonium chloride (DMOAP), or 3-(trichlorosilyl)propyl methacrylate (TCSPM) were used for the homeotropic anchoring. PFDTS and TCSPM were deposited on the surface with overnight incubation in a vacuum chamber. DMOAP was deposited on the glass surfaces from 10 minutes incubation in its 1% wt aqueous solution.

3.6. Functionalization of the Microparticles

Approximately 2% wt particle (zeolite4A) in distilled water was prepared and placed into ultrasonic bath for 10 minutes to disperse the particles. Then, 100 µl of DMOAP was added and the solution was kept in ultrasonic bath for 10 minutes again. Then, the water was refreshed by taking from the top of the bottle and adding fresh water. After this procedure was repeated for 3 times to rinse the particles with water, the water was replaced with ethanol.

3.7. Preparation of Polymeric Films

Sandwich cells were prepared with two pieces of functionalized glass slides or one glass slide and one cover slip. The spacing was set using a polyethylene film as a spacer (Saran wrap). Prepared cells were filled with LC-monomer (and chiral dopant for cholesteric LCs and microparticle for the films with particle) mixture with the help of capillary action. Then, the photopolymerization of the film was done by using Spectroline ENF-280C/FE UV lamp (365 nm; Westbury, NY) that delivered 2.5 mW.cm^{-2} at a distance of 5 cm from the light source. Sandwich cells were exposed to UV light for 30 minutes. After the polymerization, polymer films were taken from the surface of the PFDTS coated glass slides by using razor blade. For the PVA coated glass slides, sandwich cells were placed into petri dishes which were filled with distilled water and incubated overnight to dissolve PVA. When PVA that coated the surface of the glass slides were dissolved, polymer films were spontaneously detached from the surfaces. The polymer films with microparticles were not taken from cells and optical characterization was done while they are in between glass slide and cover slip.

3.8. Direct Polymerization of the Mesogenic Monomer

The mixture of photoinitiator (1-hydroxycyclohexyl phenyl ketone) and RM257 was prepared in a vial as solid mixture (without any solvent). For the planar anchoring, rubbed-glass slides and cover slips and for the homeotropic anchoring DMOAP-deposited glass slides and cover slips were placed in oven at 90℃. After the glass slides and cover slips were heated, the mixture was put on the surface of the glass slide and it was allowed that melted mixture filled the sandwich cell with the help of capillary force. After it filled the cell totally, the sandwich cell was put on a hot surface at 80℃

for 10 minutes. Then, UV light was exposed for 30 minutes for the polymerization. After the polymerization, the polymeric film was taken from the surface of the glass slide by using razor blade.

3.9. Analysis of the Shrinkage

Extraction of 5CB from the synthesized polymeric films was done using excess amount ethanol, acetone or toluene. Change in the size of the polymer films after the extraction was observed under the optical microscope and percent shrinkage was calculated based on the size of the polymer films before and after the extraction.

3.10. Optical Characterization

Optical characterizations of the films were performed using an Olympus BX50 microscope (Olympus Inc., Japan) equipped with a polarizer and an analyzer filters. Alignments of the polymers were determined from polarized micrographs in transmission mode.

3.11. Characterization of Morphology of the Polymeric Film

The morphology of the polymeric films was characterized by using QUANTA 400F Field Emission series scanning electron microscope (SEM). For the preparation of the samples, polymer films or polymers covalently bonded on glass slides were cut into a sufficient size. For the characterization of the average pore size and accessibility of the pores, nitrogen adsorption porosimetry was used. The N_2 adsorption-desorption isotherms were obtained by using Micromeritics Tristar II instruments at 77 K. The samples were prepared as covalently bonded to the substrates functionalized with TCSPM. Their alignments were checked by optical microscopy and the pore structures were checked by SEM prior to adsorption studies. The samples were degassed under vacuum at 333 K overnight. Barrett–Joyner–Halenda (BJH) model was used to estimate the average pore size of polymeric films based on the desorption data.

3.12. Thermal Analysis

Differential Scanning Calorimetry (DSC) (Shimadzu DSC-60) was used to characterize the thermal behavior of the polymer, heating and cooling was applied to the polymer between 293 K and 473 K at a rate 5 K/min. In addition, Thermal Gravimetric Analysis (TGA) (Shimadzu DTG-60H) was applied to the polymer by

heating the sample from room temperature to 873 K with a heating rate of 10 K/min and measuring the change in the weight of the sample.

3.13. Tensile Tests

Tensile tests were performed using a Shimadzu Autograph AG-100 KNIS MS universal tensile testing instrument. The samples were prepared in the form of films in dimensions of 30 mm gauge length, 10 mm in width and 120 μm in thickness following ASTM standards ASTM-D882. The tests were performed in a strain rate of 3 mm/min at room temperature.

3.14. Filtration

Filtration tests of the polymeric films with area of 1 cm^2 were performed in filter modules connected to the syringe as a simple dead-end system. A transmembrane pressure difference of 1 bar was applied during filtrations by putting weight on the top of the syringe. Ethanol, water, solution of bovine serum albumin (BSA) in phosphate-buffered saline (1g/L) and solution of 200 nm- in diameter sulfate PS in water were used as feed and permeate was collected with the volume of 2 ml with respect to time to calculate flux (L/m^{2}h) and rejection percentage. In order to obtain the concentration of BSA in the permeate, UV-visible spectrophotometer (Shimadzu UV-1601) was used.

3.15. Gas Permeation Test

Gas permeability tests of the polymeric films were performed by using constant volume method. In order to analyze the gas permeation properties of the polymeric films with area of 1 cm^2, they were placed into a stainless steel membrane module, then nitrogen and carbondioxide were used as feed. The module was placed in a cell to keep the temperature as 35°C during the tests. Transmembrane pressure was applied as 1 bar and pressure of the permeate side was recorded with respect to time by using a pressure transducer. Then, the permeability values were calculated by using the data where the pressure difference exhibited linear dependency on time.

CHAPTER 4

RESULTS AND DISCUSSIONS

4.1. Synthesis and Characterization of the Polymeric Films with Specified Internal Structure

In this chapter, the studies on the synthesis, characterization on investigation of the applications of polymeric materials templated from liquid crystals are presented.

4.1.1. Determination of the Alignment of the Polymeric Network

The mixture of a reactive mesogen, 4-(3-acryloyloxypropyloxy) benzoic acid 2-methyl-1, 4-phenylene ester (RM257) and a non-reactive mesogen, 4-cyano-4′-pentylbiphenyl (5CB) was prepared (Figure 4.1) and sandwiched between two functionalized glass surfaces that mediate a determined alignment of the mesogens. Then, the mixtures were photopolymerized using a UV-light and the sandwich cells were detached to obtain free standing polymeric films (Figure 4.1b). Following this procedure, polymeric films of size in the order of 1-10 cm^2 (Figure 4.1c) were able to synthesized. As functionalized surfaces, the rubbed-polyvinylalcohol (PVA) surfaces and perfluorodecyltriethoxysilane (PFDTS)-deposited glass surfaces were used for uniform planar alignment and the homeotropic alignment of mesogens, respectively. Since the surfaces with different chemical functionality were used during the synthesis, it was possible to provide control over the alignment of the resulting polymeric network as determined by optical microscopy. Figure 4.1d shows the polarized light optical micrographs of two separate 20 µm-thick films synthesized from 20% wt RM257 between two surfaces of planar alignment (top row) and two surfaces of homeotropic alignment (bottom row). The films synthesized between rubbed-PVA surfaces exhibit dark appearance under polarized light when the average alignment of the LCs in the direction of one of the polarizers. When the film was rotated 45 degrees, the appearance of a bright transmitted light was consistent with the uniform planar alignment. The films synthesized between PFDTS-coated surfaces did not exhibit such an angle-dependent appearance under polarized light and the cross pattern was visible

23

in the conoscopic images, which are two evidences consistent with a uniform homeotropic alignment of the LCs.
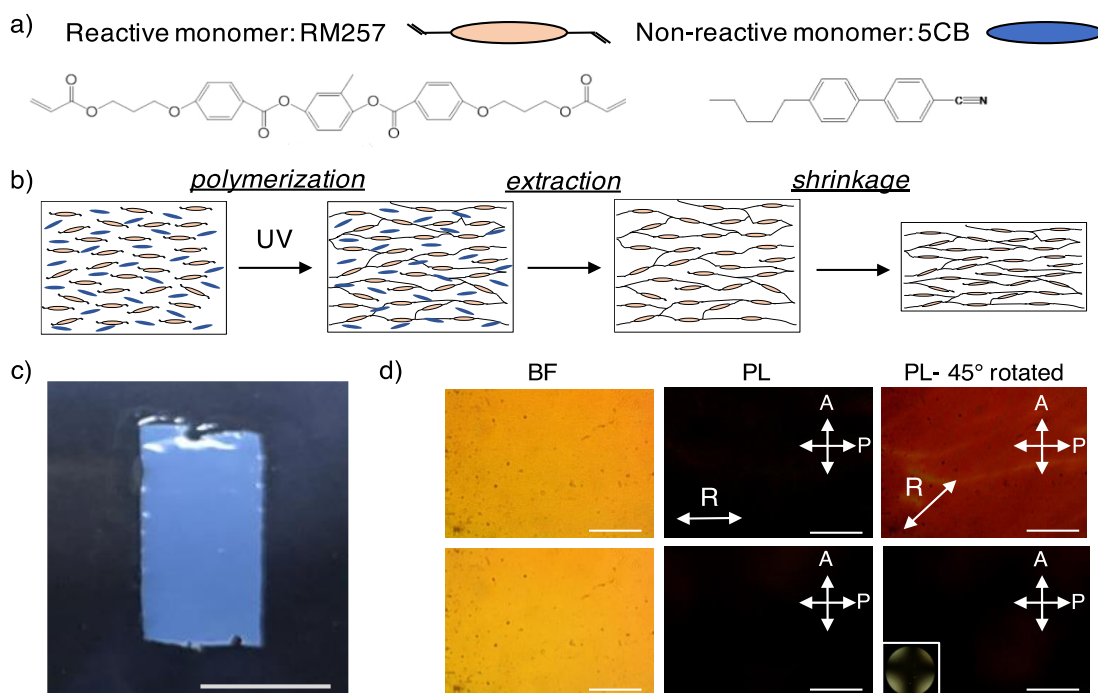
Figure 4.1 (a) Molecular structures of reactive mesogen 4-(3-acryloyloxypropyloxy) benzoic acid 2-methyl-1, 4-phenylene ester (RM257) and non-reactive mesogen 4-cyano-4′-pentylbiphenyl (5CB) used in this study. (b) Schematic illustration of the experimental procedure showing polymerization of RM257 and extraction of 5CB. (c) Photograph of an 80 μm-thick polymeric film synthesized from 20% wt RM257 and 80% wt 5CB with planar anchoring. Scale bar: 1 cm (d) Bright field (left) and polarized (middle and right) light micrographs of the polymeric films (20% RM257) with planar (top row) and homeotropic (bottom row) anchoring. Inset showing conoscopic image of the film. Scale bars: 50 μm

Before we used the rubbed-polyvinylalcohol (PVA) surfaces and perfluorodecyltriethoxysilane (PFDTS)-deposited glass surfaces, bare rubbed glass surfaces and octadecyltrichlorosilane (OTS)-deposited glass surfaces were used for the uniform planar alignment and the homeotropic alignment of mesogens, respectively.

As shown in Figure 4.2, the alignment of the liquid crystal was provided as requested with both of these glass slides.
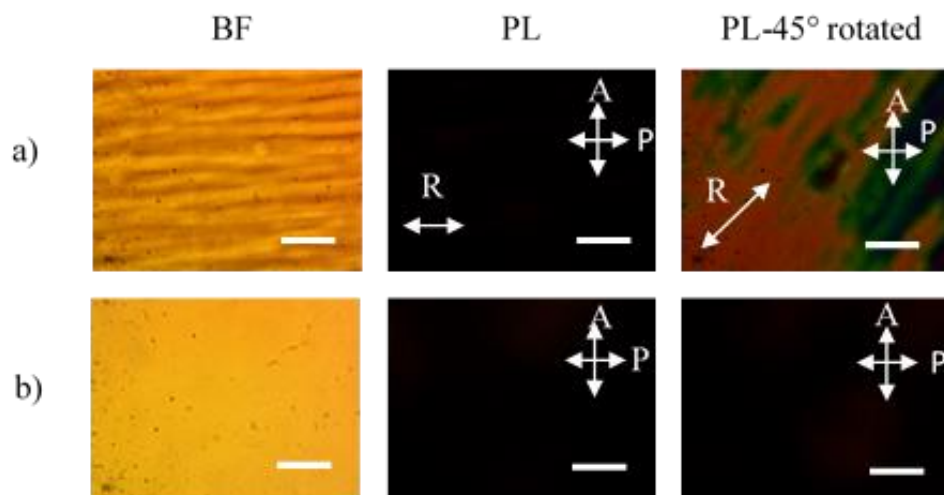
Figure 4.2 Bright field (left) and polarized (middle and right) light micrographs of the polymeric films (20% RM257) synthesized on (a) rubbed-bare glass slide and (b) OTS deposited glass slide. Scale bar: 50 μm

However, when we tried to detach the glass slides to take the polymeric films, obtaining the polymeric films from these surfaces was more challenging than rubbed-PVA and PFDTS. As it can be seen from Figure 4.3, we could not obtain the polymeric film as a whole when rubbed-bare glass slide and OTS-deposited glass slide were detached. Therefore, we decided to use rubbed-PVA coated glass slide and PFDTS-deposited glass slide for planar and homeotropic anchoring, respectively.
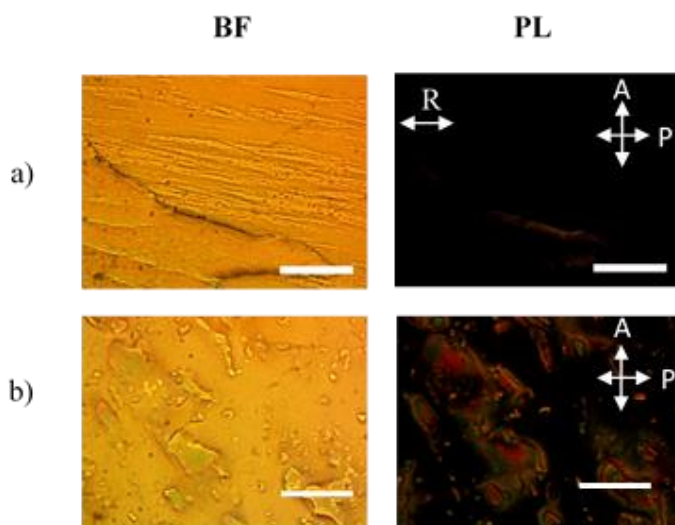
Figure 4.3 Bright field (left) and polarized (right) light micrographs of the polymeric films (20% RM257) on (a) rubbed-bare glass slide and (b) OTS-deposited glass slide. Scale bars: 50 μm

For the films which were synthesized between rubbed-PVA coated glass slides, distilled water was used to dissolve PVA layer, which is sacrificial layer, so the films were obtained properly. In the case of PFDTS-deposited glass slide, razor blade was used to remove the film from the surface of the glass slides. In order to evidence that using the razor blade did not affect the alignment of the polymers, the alignment of polymeric films was checked by using polarized optical microscope before and after removal of the film using the razor blade. As it can be seen in Figure 4.4, the alignment of the polymeric films synthesized between PFDTS-deposited glass slides was retained during the procedure of obtaining the polymeric film.
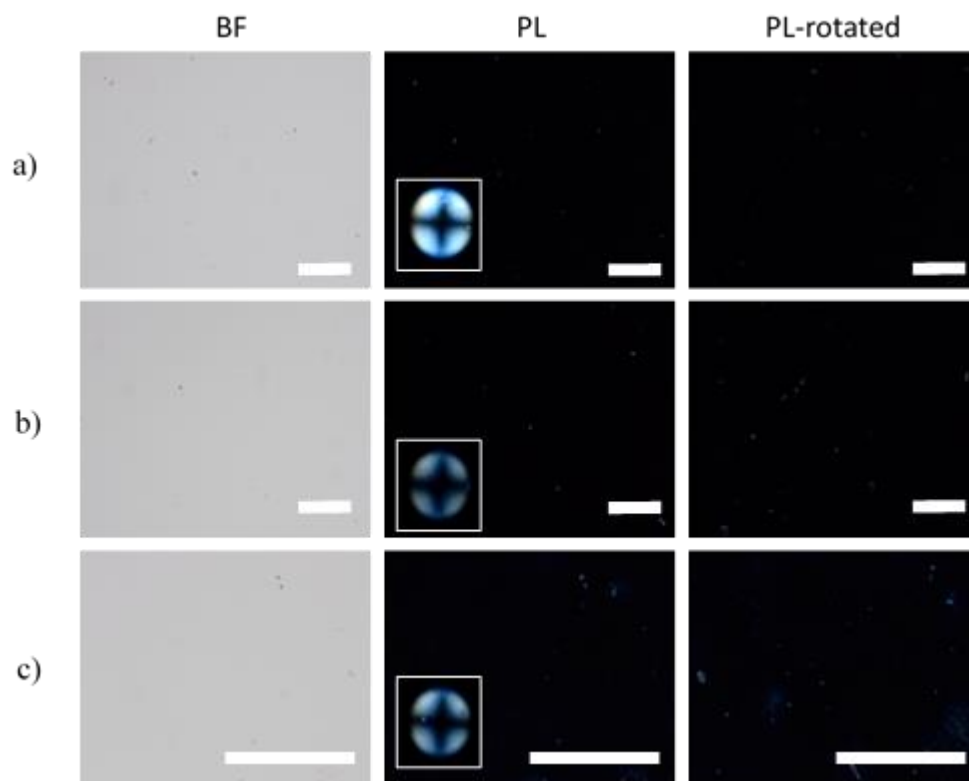
Figure 4.4 Bright field (left) and polarized (middle and right) light micrographs of the polymeric films (20% RM257) synthesized between PFDTS-deposited glass slides (a) before polymerization (b) after polymerization and (c) after the application of razor blade Scale bars: 500 µm.

4.1.2. Effect of the Thickness on the Alignment of the Polymeric Films

As summarized in the Introduction section, thickness plays an important role in the uniform alignment of LCs. In order to investigate the effect of the thickness on the alignment of the polymeric films. The films that were synthesized with different thickness (20, 40, 80 and 160 µm) were analyzed by using optical microscope (Figure 4.5).
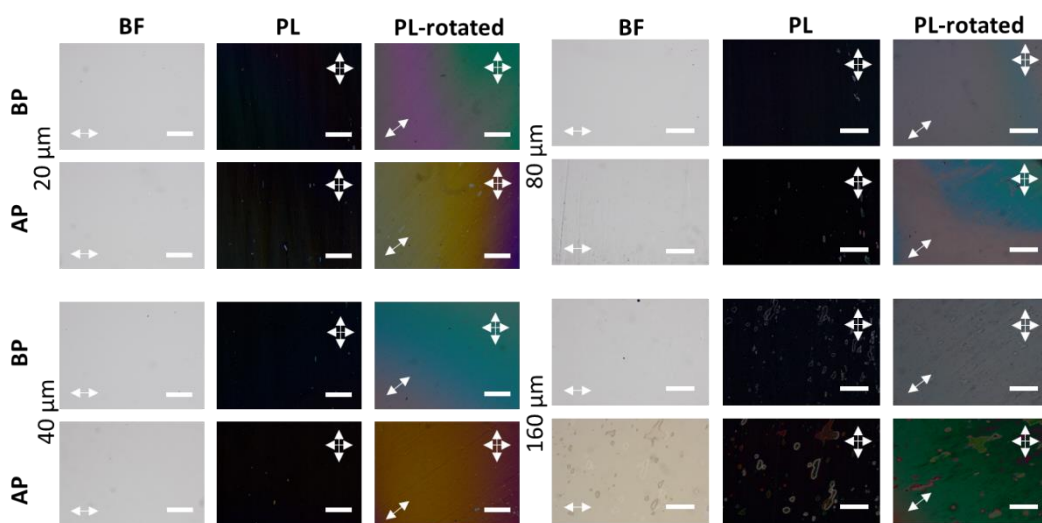
Figure 4.5 Bright field (BF) and polarized light (PL) micrographs of the polymeric films (20% RM257) synthesized with planar anchoring and thickness of 20, 40, 80 and 160 μm. Scale bars: 200 μm

Although the thickness of the polymeric films caused a difference in the colors of the sample between crossed polarizers when rotated by 45° as expected[88] , we did not observe any effect on the alignment of the polymers as shown in Figure 4.5. Therefore, it can be said that the alignment of the polymeric films can be controlled at least in the range of 20-160 μm.

4.1.3. Thermal and Chemical Characterization of the Polymers

After the polymerization step, we extracted the unreacted mesogens from the polymer using an excess amount of ethanol. In order to evidence that the unreacted part (mainly 5CB) was removed completely from the polymer, different analysis methods were used. With differential scanning calorimetry (DSC) (Figure 4.6), it was demonstrated that the unreacted part could be separated completely from the polymer.
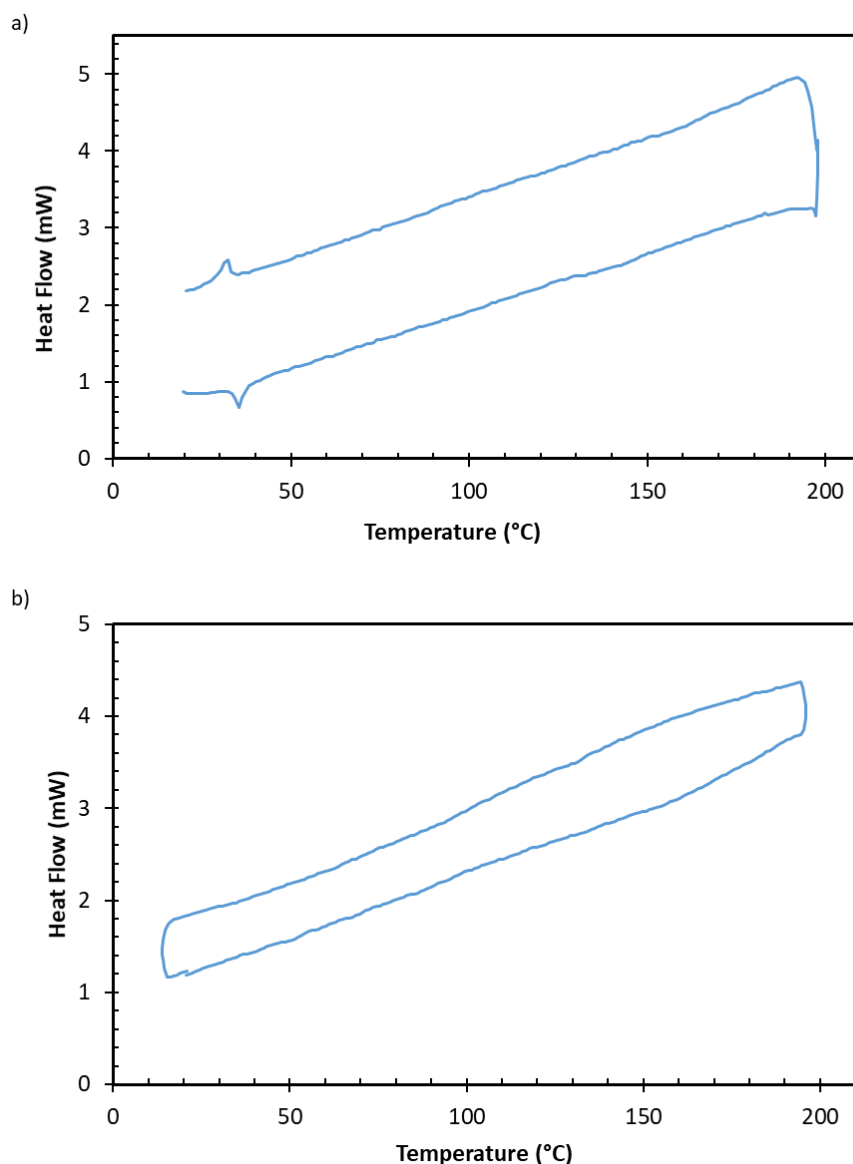
Figure 4.6 Differential Scanning Calorimetry results of polymeric film synthesized from 20% RM257, 80% 5B by weight (a) as polymerized (b) after extraction of (5CB) (10 °C/min heating and cooling)

As seen from Figure 4.6, the peak that came from the nematic-isotropic transition of 5CB (nearly at 35°C) disappeared after the extraction of the unreacted part, which is mainly 5CB. In addition, thermogravimetric analysis (TGA) (Figure 4.7) of the extracted films evidenced that the mass of the polymer left was consistent with the amount of the reactive monomer initially mixed with 5CB.
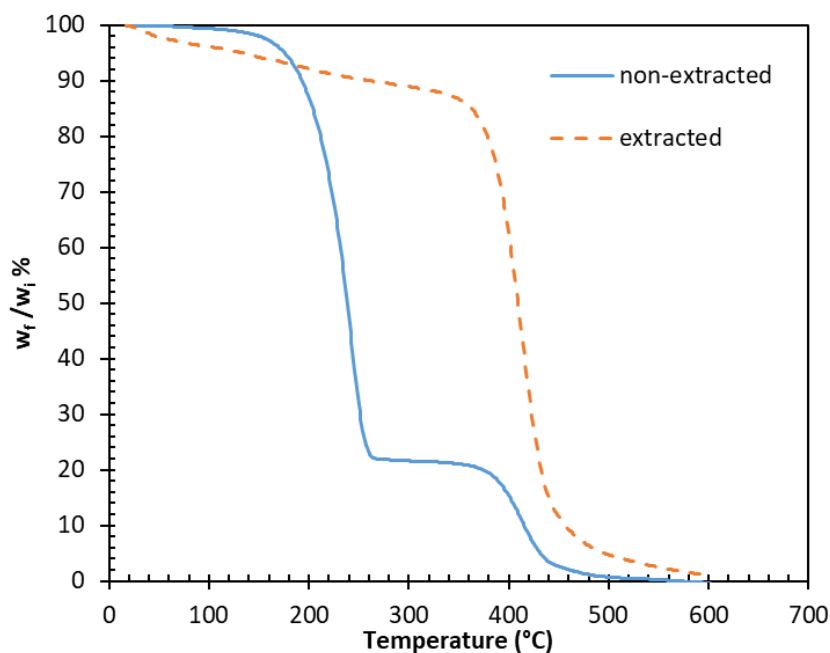
Figure 4.7 Thermal gravimetric analysis (TGA) of polymeric film synthesized from 20% RM257, 80% 5B by weight as polymerized (solid line) , after extraction of (5CB) (dashed line) (10 °C/min heating)

In addition, the FTIR data shown in Figure 4.8 were collected to provide information of the chemical structure of the synthesized polymer and the removal of 5CB from the polymer after extraction. The peak observed around 2200 cm^{-1} is the peak corresponding to the nitrile group present in 5CB, but not in RM257 (shown as monomer in the figure). This peak was present in the FTIR spectra of the 20% wt RM257 in 5CB mixture before and after polymerization, and it diminished after extraction of 5CB from polymer using ethanol. This data, along with the TGA and DSC data supported the complete removal of 5CB from the polymer after extraction. In addition, the peak around 1700 cm^{-1}, which was present in the FTIR spectra of monomer, mixture before and after polymerization and the polymer after extraction, originates from the stretching of C=O bond present in RM257, but not in 5CB. Besides, the multiple peaks between 1000-1300 cm^{-1} originates from stretching of C-O present in the ester groups of RM257. Overall, the signatures in the FTIR spectra satisfies the chemical structure of RM257 and consistent with the removal of the 5CB from polymer after extraction. We also note that these data were consistent with a similar analysis done in the literature.[89]
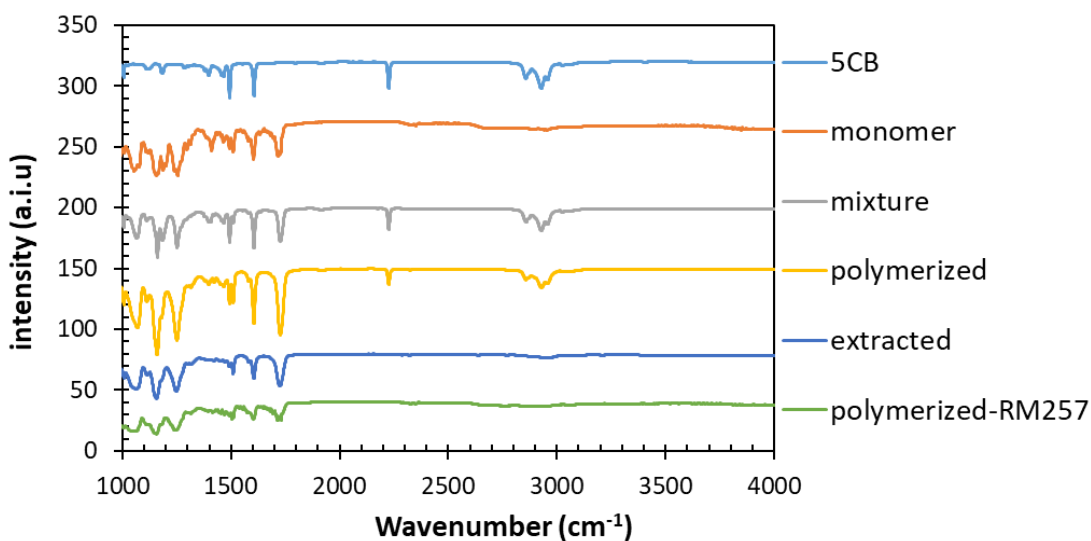
Figure 4.8 FTIR spectra of pure 5CB, monomer (RM257), before and after the polymerization of the mixture of 20% RM257 and 80% 5B by weight, after the extraction of the unreacted part and polymerized pure RM257.

4.1.4. Analysis of the Anisotropic Shrinkage of the Polymer

After the extraction of the unreacted mesogens and drying of the solvent, an anisotropic shrinkage of the films was observed. Figure 4.9 shows the micrographs of the 20 μm-thick films synthesized from 20% wt RM257 in 5CB before and after the extraction of the unreacted mesogens. Figure 4.9a shows the micrographs of a piece of a film synthesized between surfaces of planar anchoring, where the nematic director is towards the short axis (shown as **n** in the figure). A substantial shrinkage of the film generated after the extraction in a direction perpendicular to the director is evident in the micrographs. In addition, the alignment within the film was preserved after the extraction step as evidenced by the polarized light micrographs. In order to provide more evidence on the director-dependent shrinkage of the films, we performed the same optical characterization to two more films synthesized with different alignment conditions at the two surfaces (Figure 4.9 b and c). Consistent with the observation of a nematic director-dependent shrinkage, we observed isotropic shrinkage of the films that were synthesized between surfaces of homeotropic anchoring and a curling of the film into a cylindrical shape when the films were synthesized between surfaces mediating homeotropic-planar hybrid anchoring at the two sides. Cylindrical shape

31

was formed due to a shrinking imbalance between the two surfaces. These observations led us to perform characterizations on the structure of the films synthesized from liquid crystalline molecular templates since the shrinking behavior of the materials is usually attributed to the nanoscopic features of the materials, which we characterize in detail below.
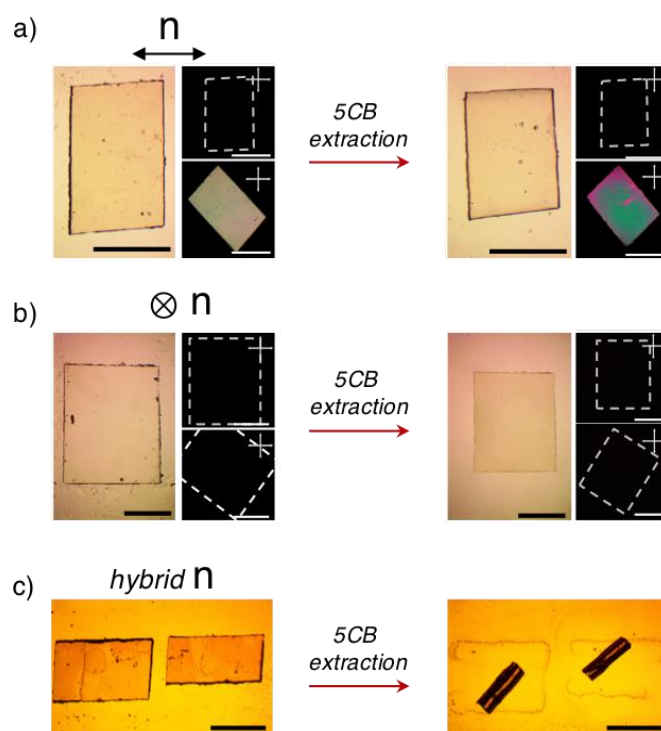
Figure 4.9 Optical micrographs of 40 μm-thick polymeric films synthesized from mixtures of 20% RM257 and 80% 5CB by weight. Brigthfield and polarized optical micrographs of the films with **(a)** planar anchoring, **(b)** homeotropic anchoring, and **(c)** hybrid anchoring are shown before (left column) and after (right column) extraction of 5CB. n indicates the nematic director. Crossed lines in figures indicate the direction of the polarization of the polarizer and analyzer. Dashed line in the images were drawn to indicate the boundaries of the films. Scale bars: 500 μm.

We quantified the shrinkage of the polymers in a direction parallel and perpendicular to the nematic director as a function of the concentration of the reactive mesogens. Figure 4.10 shows the shrinkage of the polymers with respect to their initial size as a function of the monomer concentration. A linearly decreasing percent shrinkage of the

films from 45% to 25% was observed perpendicular to the director as the RM257 content of the films were increased from 10% to 30% wt, whereas nearly 7% shrinkage was observed in the direction parallel to the director, independent of the RM257 content of the films. This shrinking behavior is consistent with the previous observations in polymerized LC droplets by Wang et al.[3] Along with these observations, when the changes in the volumes of the films were calculated from the measured dimensions, we observed a linear dependency of the final to initial volume ratio (V_f/V_i) as a function of the RM257 content (detailed below).
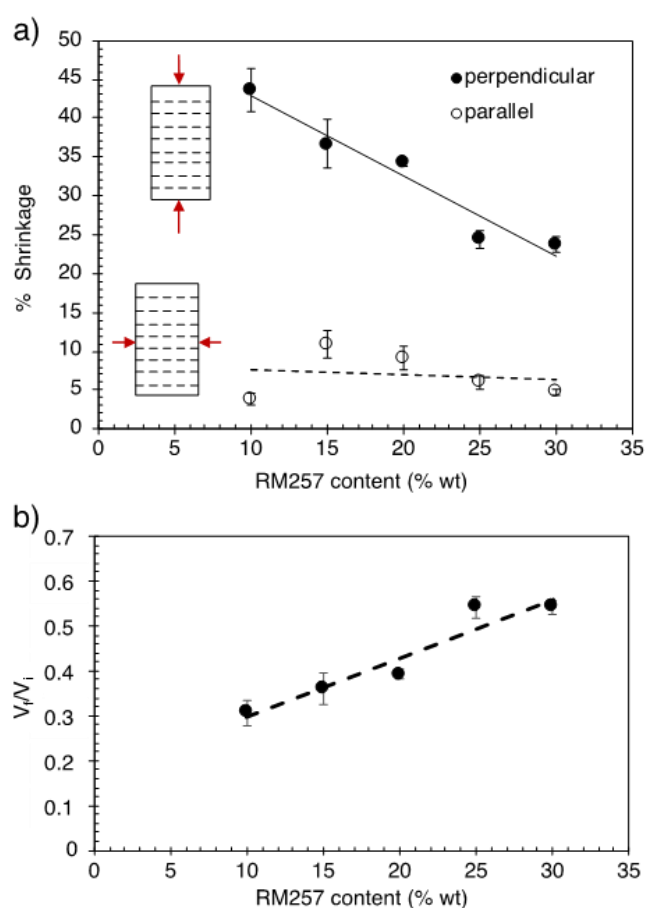
Figure 4.10 (a) Percent shrinkage of the polymeric films along (open symbols) and perpendicular (filled symbols) to the director as a function of the concentration of RM257 after extraction of 5CB. (b) Ratio of volumes of films before (V_i) and after (V_f) extraction of 5CB as a function of the concentration of RM257. Analysis were done on films with thickness of 160 μm.

When the films were placed in the solvent for extraction, we did not observe an observable shrinkage of the films even after overnight incubation of the films in the solvent (although the solvent dissolved the entrapped unreacted mesogens). Interestingly however, a substantial shrinkage occurred immediately after the films were dried out from the solvent used for extraction. Therefore, the two observations, (*i*) a shrinkage of the films that correlate with the reactive mesogen content (function of RM257 content Figure 4.10 b) and (*ii*) the occurrence of the shrinkage immediately and only after the films were dried from the extraction solvent, evidences an incorporation of porosity within the films, which close after drying following the extraction. We note that, supporting this hypothesis, we observed swelling of the dried films back to their initial dimensions when exposed to toluene and acetone, the solvents that we found to plasticize the polymerized RM257 (Figure 4.11c,d). However, no substantial effects of water or ethanol exposure on the size or shape of the films were observed after exposure (Figure 4.11a,b). We relate this behavior to the reversible closure of the pores incorporated to the polymer structure after extraction.
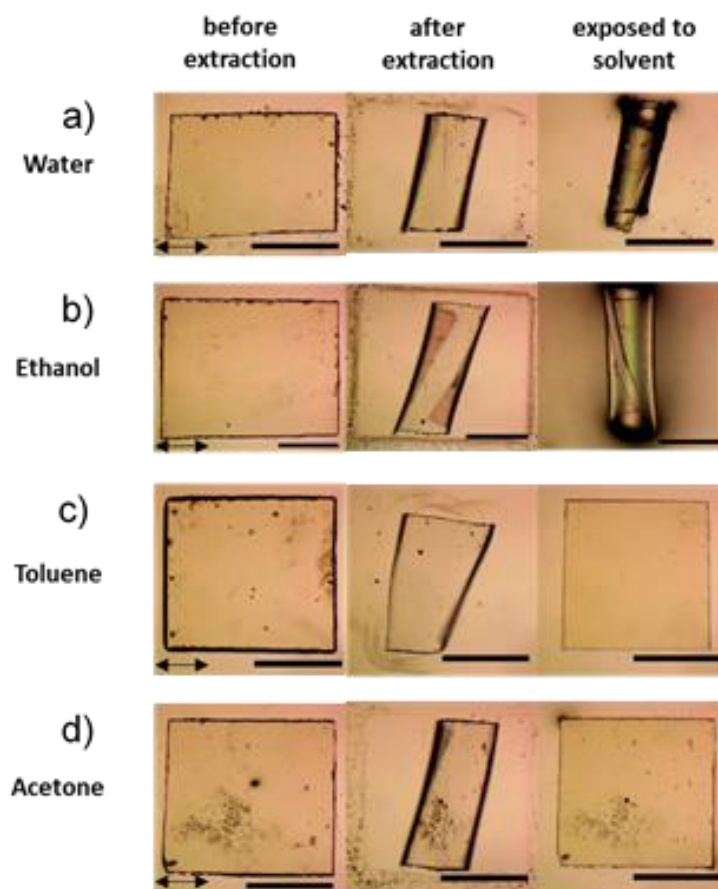
Figure 4.11 Brightfield optical micrographs of polymeric films synthesized from mixtures of 20% RM257 and 80% 5CB by weight showing the changes in the shapes of the films when exposed to (a) water, (b) ethanol, (c) toluene, and (d) acetone after extraction of 5CB. Micrographs were collected before extraction of 5CB (left column), after extraction of 5CB (middle column), and after exposed to the indicated chemicals (right column). Scale bars: 100 μm.

4.1.5. Incorporation of the Pores into Polymeric Structure

When we examined the scanning electron microscopy (SEM) images of the films after extraction, we observed rough surfaces both for the films synthesized between PVA-coated and PFDTS-coated glass surfaces (Figure 4.12a, b). Since the PVA or PFDTS-coated glass surfaces would not potentially incorporate such roughness to the surfaces of the polymers, we hypothesize the rough surface features evident in the SEM micrographs to result from the closure of the pores within the films.
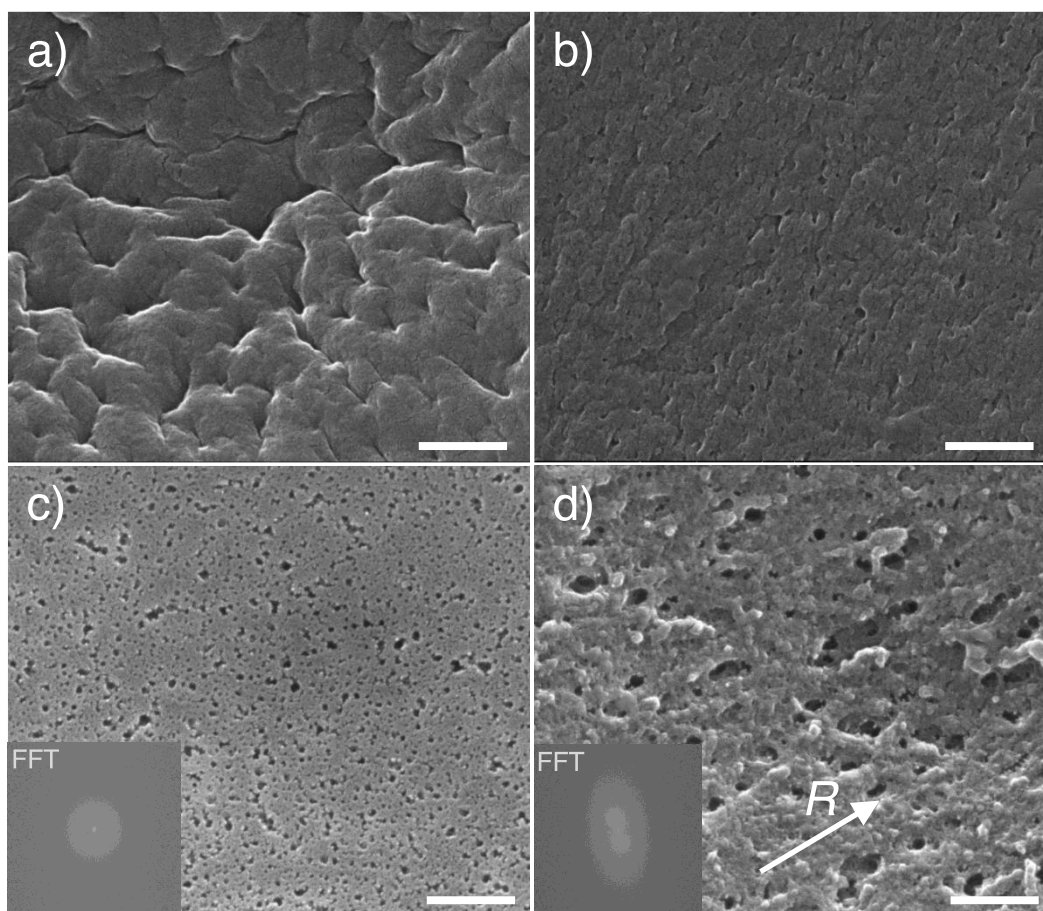
Figure 4.12 Scanning electron micrographs of the polymeric films synthesized from 20% RM257 and 80% 5CB by weight. (a) and (b) shows the micrographs of the homeotropic and planar films, respectively, after extraction of 5CB. (c) and (d) shows the micrographs of the films covalently bonded to the underlying TCSPM substrate and top surfaces synthesized when contacting surfaces mediating (c) homeotropic, and (d) planar anchoring of mesogens. Inset images show FFT of the corresponding SEM images. *R* shows the azimuthal anchoring of the mesogens at the top surface. Scale bars: 500 nm.

We prevented the films from shrinking after the extraction by covalently attaching the films to the underlying substrate to maintain the hypothesized porous morphology after extraction. For the reactive underlying substrate, we functionalized the glass surfaces with acrylate-terminated silane molecules, 3-(trichlorosilyl)propyl methacrylate (TCSPM), and synthesized the polymer via polymerization of the RM257-5CB mixture on the surfaces (Figure 4.13a). When this procedure was followed, we did not

observe polymer to detach from the TCSPM-functionalized substrate and did not shrink after extraction of the unreacted mesogens or drying of the films from the solvent used for extraction. We found that the prevention from shrinkage was independent of the top substrates contacting the polymer during synthesis (either PFDTS-functionalized or PVA-coated glass), which were removed after polymerization. These observations suggested the pores to maintain their openings after the extraction step. When the SEM micrographs of the extracted films covalently attached to the TCSPM substrates were compared to the micrographs of the shrunk films, the pores were evident in the covalently attached films (Figure 4.12c and d). This observation is consistent with our above hypothesis that the shrinkage of the films was due to the destruction of the pores.
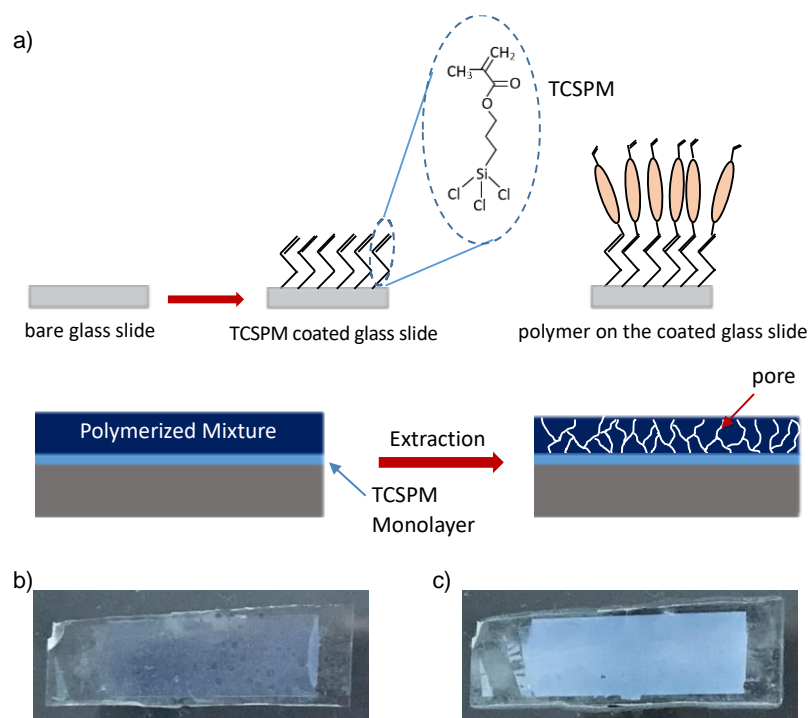
Figure 4.13 (a) Schematic illustration of the procedure followed during the synthesis of polymeric films covalently bonded to the contacting 3-(trichlorosilyl)propyl methacrylate, TCSPM-coated surfaces. Top row shows the functionalization of the glass surfaces with TCSPM, bottom row shows the representation of the extraction of the polymeric film coated on TCSPM surface. Photographs of the films after polymerization and after extraction are shown on (b) and (c), respectively.

Therefore, by functionalization of the glass surfaces with TCSPM, it became possible to prevent the shrinkage of the polymeric films, so the pores were stayed as opened in the polymeric structure.

4.1.6. Mechanical Characterization of the Polymeric Film

Destruction of the pores could be possible if the polymer network is soft enough to deform. To provide an evidence, we measured the elastic modulus of the polymers. We performed tensile tests to the films synthesized between rubbed-PVA coated surfaces along and perpendicular to the director.
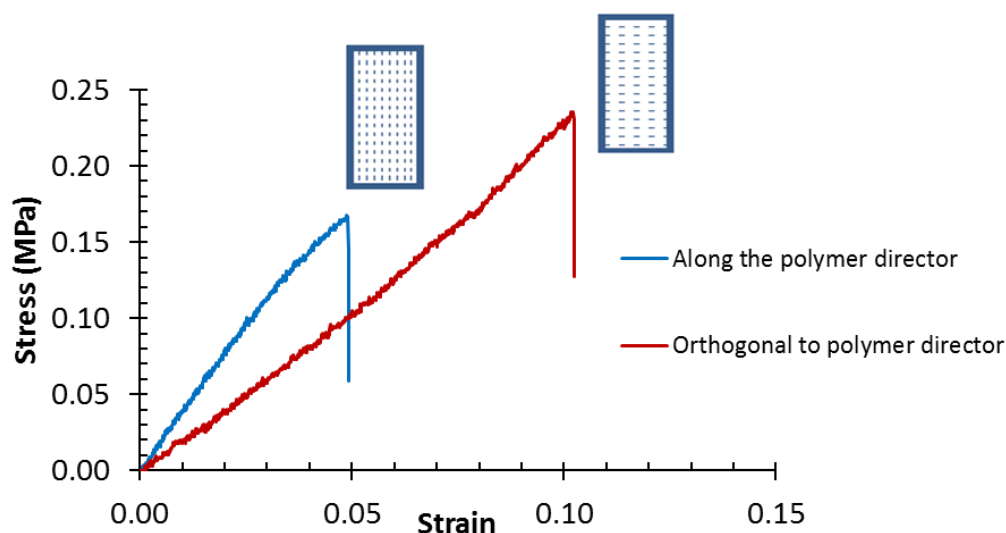
Figure 4.14 Stress-strain diagram of the polymeric films in tensile mode. Stress was applied either in a direction along or orthogonal to the director. The films were synthesized from 20% RM257 and 80% 5CB by weight.

The films exhibited elastic moduli of 5.9 ± 1.4 MPa along the director, and 1.4 ± 0.4 MPa perpendicular to the polymer director (Figure 4.14). These values are in the range of the soft tissues, that could easily deform.[90]

4.1.7. Characterization of the Microstructure of Pores Incorporated into Polymeric Film

We used SEM and nitrogen adsorption isotherms to reveal details about the pore structure of the film. We prepared polymeric films of varying RM257 content between TCSPM-PFDTS substrates and collected SEM micrographs shown in Figure 4.15a. The films exhibited different morphologies and pore sizes depending on their RM257 content. Films of 10% wt RM257 exhibited a fibrous structure with large interconnected pore structure, whereas films prepared from RM257 concentration in the range 20-40% wt, exhibited more disconnected, smaller size pores. We characterized the pore size distributions based on the collected SEM micrographs as shown in Figure 4.15b. As expected, the width of the pore size distribution was substantially wider for the films of 10% wt RM257 compared to the other films. The average sizes of the pores calculated from these histograms were found to be linearly dependent on the RM257 content of the films. The average pore diameter decreased from 40 nm to 10 nm as the RM257 content was increased from 10% to 40% by weight. We also note that the average pore diameters in the films were similar to the average pore diameters incorporated into the polymeric particles synthesized from aqueous emulsions of LC-monomer mixtures.[3] Consistent with these SEM characterizations, the average pore sizes calculated from nitrogen sorption isotherms were found to be 29.6 ± 2.8 nm and 24.4 ± 0.7 nm for the films synthesized from 20% wt RM257 and 40% wt RM257, respectively. Nitrogen sorption isotherms also showed that the mesoscale pores evident in the micrographs were accessible to the external species.
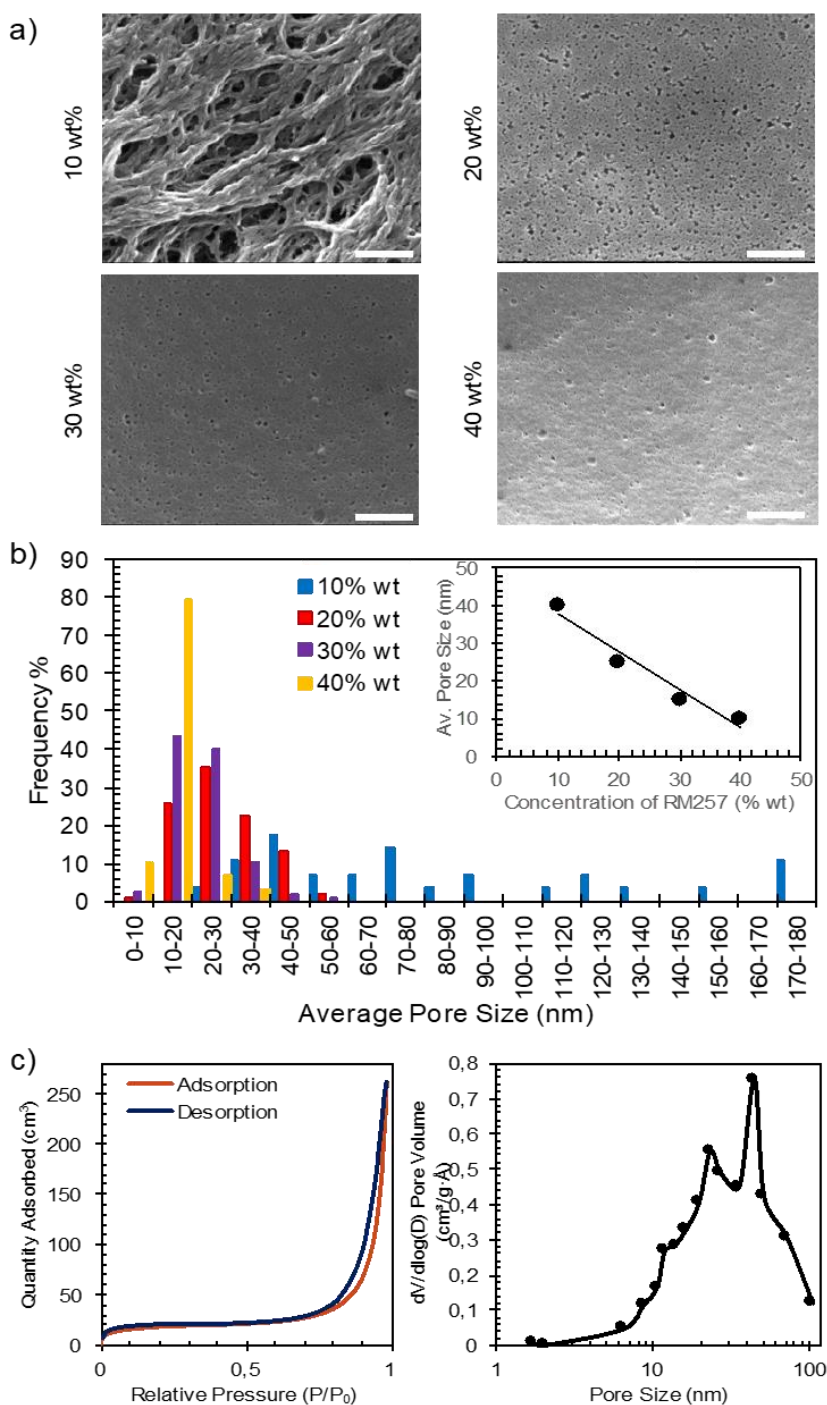
Figure 4.15 Characterization of the pore sizes of the polymeric films synthesized from mixtures of RM257 and 5CB. (a) Scanning Electron Micrographs of the polymeric films synthesized form different concentrations of RM257. Scale bars: 500 nm. (b) Pore size distribution of the films measured using SEM micrographs, (c) Nitrogen sorption isotherm (left) and the calculated pore size distribution using BJH theory (right) of the film synthesized from 20% RM257 and 80% 5CB by weight.

4.1.8. Prevention of the Shrinkage by Ordering Symmetry of Chiral Nematics

In addition to the covalent bonding to the surfaces, prevention from shrinkage could also be maintained by placing a restriction through ordering symmetry of chiral nematics. Since the shrinking behavior of the films were director-dependent, and more preferential in a direction perpendicular to the local nematic director, the ordering symmetry of chiral nematics, when chemically crosslinked, would prevent the shrinkage in the nematic director. Figure 4.16 shows an SEM of a film synthesized from an LC mixture with 20% wt chiral dopant, S-811, between rubbed-PVA surfaces causing planar anchoring. The image is the surface of a free-standing film (not bonded on the underlying substrate) after extraction of the unreacted mesogens. The pores are evident in the images, which are in the range 158 ± 66 nm. This result and generalization approach also explained the incorporation of porosity to the polymeric films synthesized from hydrogen-bonded cholesteric networks after evaporation of the templating material.[91,92]
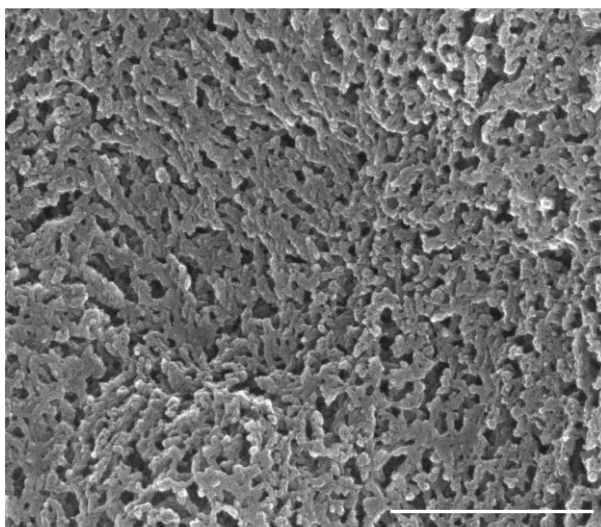
Figure 4.16 Scanning electron micrograph of the surface of a free-standing, 20 μm-thick polymeric film synthesized from 20% RM257, 20% chiral dopant and 60% 5CB by weight (after the extraction of 5CB with the excess amount of ethanol). Scale bar: 2 μm.

The collapse of the pores can also be prevented by placing the films between two surfaces that provide a physical constraint (such as between two o-rings). An example of this is shown below along with a functional property of the films.

4.1.9. Determination of the Alignment of Pores in Polymeric Film

When the pore structures of the 20% wt RM257 films synthesized between TCSPM-PFDTS or TCSPM-PVA sandwich cells were compared, a substantial difference in the morphology of the pores is evident in the SEM micrographs (Figure 4.12c,d and Figure 4.14). The films synthesized between TCSPM-PFDTS cells exhibit pores which had no substantial directionality along the surface plane, whereas the films synthesized between TCSPM-PVA cells exhibit an overall in-plane orientation in the rubbing direction of the PVA substrate as shown in Figure 4.17.
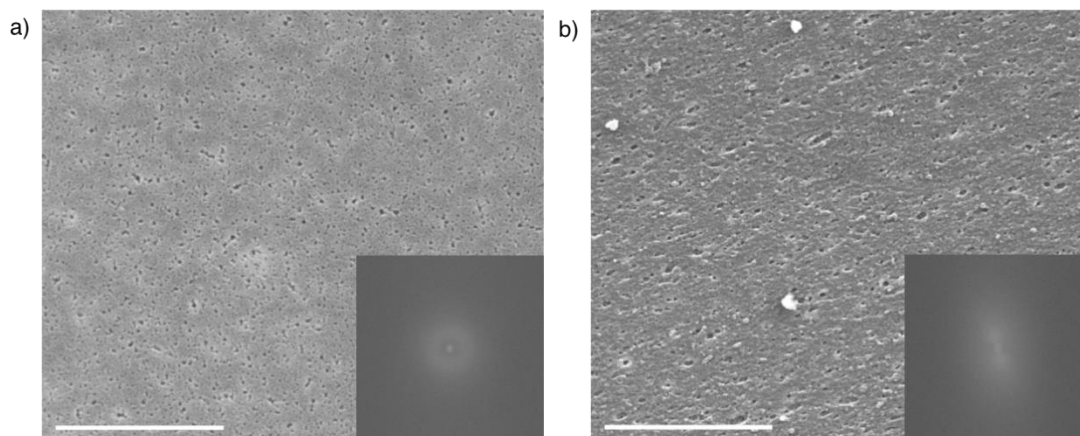
Figure 4.17 Scanning electron micrograph of the surface of 20 µm-thick polymeric films synthesized from 20% RM257 and 80% 5CB by weight. (a) film synthesized between TCSPM-PFDTS (homeotropic) substrates (b) film synthesized between TCSPM-PVA (planar) substrates. Insets shows FFT of the corresponding images. 5CB was extracted by using excess amount of ethanol. Scale bars: (a) 2 µm, (b) 5 µm

These observations were further supported by the Fourier Transform of the images included as insets to the corresponding SEM micrographs. If the orientations of the pores were determined by the nematic director, we expected the films synthesized between TCSPM-PFDTS to exhibit an overall orientation of the pores in a direction

orthogonal to the film surfaces. Supporting this expectation, the SEM micrographs of the cross-section of the homeotropic films synthesized between TCSPM-PFDTS substrates indeed exhibited a pore directionality orthogonal to the film surface planes as shown in Figure 4.18a. Moreover, such a directionality in absent in the cross-section images of the films synthesized from chiral LC mixture (Figure 4.18b). FFT of the images shown in insets are also supporting this anisotropy.
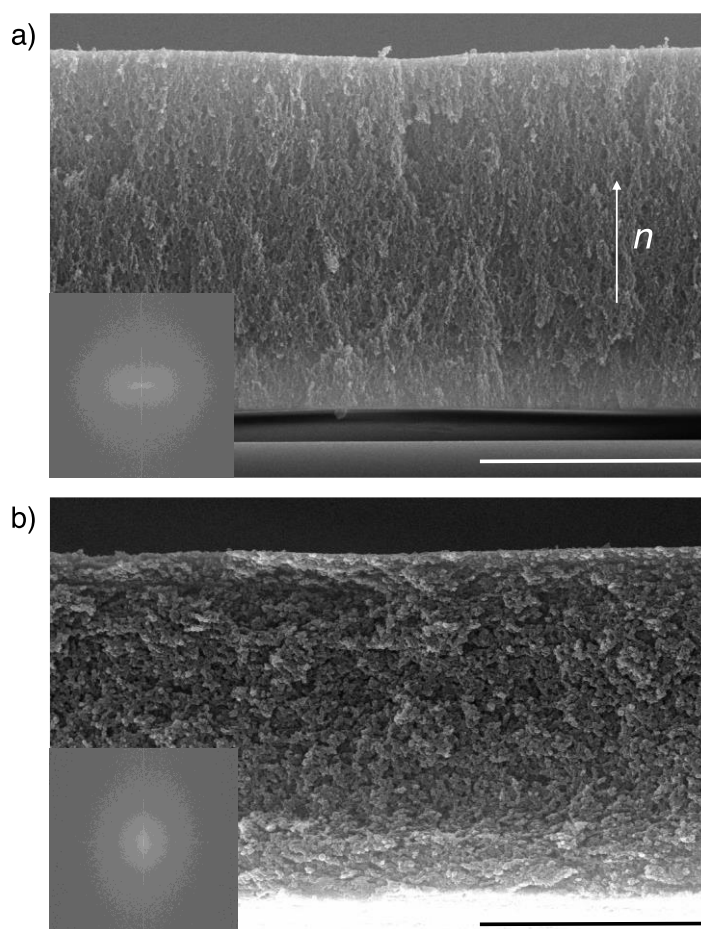
Figure 4.18 Scanning electron micrographs of the cross-section of 20 μm-thick polymeric films synthesized from (a) 20% RM257 and 80% 5CB by weight between TCSPM-PFDTS substrates, and (b) 20% S-811, 20% RM257 and 60% E7 by weight between PVA substrates. *n* showing nematic director. The film shown in (a) is covalently bonded to the underlying substrate, whereas the film in (b) is a free-standing film. The PFDTS and PVA substrates were removed for extraction of the films. Scale bars: 10 μm. Insets show the FFT of the corresponding images.

4.1.10. Use of the Polymeric Films as Ultrafiltration Membranes

We have evidenced that the films synthesized from LC templates exhibit mesoscale pores in a direction determined by the nematic director during the synthesis. We hypothesize that we can employ this control over the microstructure of the films to significantly improve the performance of the films that are to be used in chemical processes. Lastly, we showed a demonstration of a functional property of the films synthesized from liquid crystals that provide advantageous mass transfer properties. The accessibility of the pores and an average pore size in the order of 10 nm suggests the use of the films as ultrafiltration membranes. However, a film is needed to be defect (hole)-free in order to be used as a membrane. As a conceptual illustration, we prepared films from 20% wt RM257 in 5CB with homeotropic and planar ordering. We prevented the films from shrinkage and measured the permeances of ethanol, water, and aqueous solutions of bovine serum albumin (BSA) and 200 nm-in-diameter polystyrene (PS) particles. In addition, we calculated the rejection of BSA and PS particles for the quantification of the separation performance. The motivation behind this set of experiment was three folds; (*i*) to examine whether there are defects (holes) within the polymeric films that were not quantified in N_2 adsorption, optical or electron micrographs, (*ii*) to demonstrate that the directions of the pores has an influence on the permeances through the films, and (*iii*) to examine whether the pores can serve as a separation medium for molecular-level species (1-10 nm).

As shown in Figure 4.19, during the filtration of PS particles with 200 nm in diameter from water, we did not observe any permeated PS particles through the films, which suggests that there were no holes within the films that would allow particles in the 100 nm range to permeate.
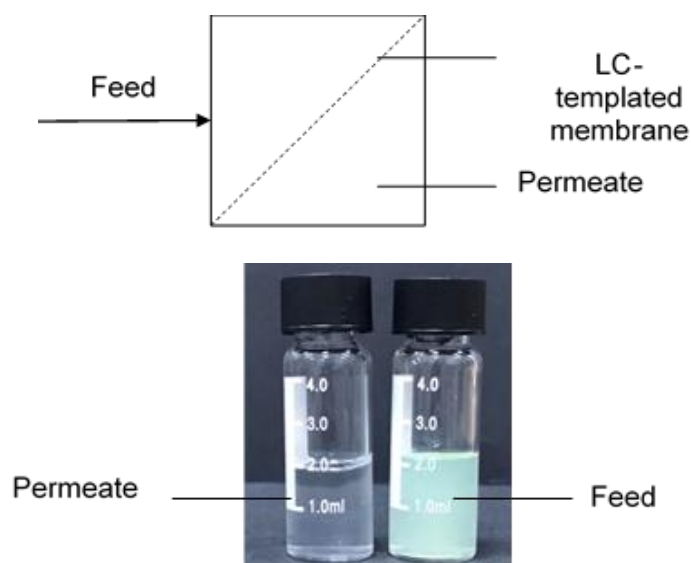
Figure 4.19 (a) Schematic representation of the filtration and (b) Photograph of vials with the permeate on left hand side, feed solution (200 nm- in diameter sulfate PS in water solution) on the right.

Second, when the permeances of water and ethanol were compared, we observed up to two orders of magnitude higher permeances through films with pores orthogonal to the surfaces compared to their horizontal counterparts. As shown in Table 4.1, ethanol permeance were observed to be 24.7 ± 4.0 L/m^2.h.bar for planar films, whereas it was observed to be 602.8 ± 178.1 L/m^2.h.bar for homeotropic films. Similarly, water permeance were observed to be 1.6 ± 0.1 L/m^2.h.bar for planar films, whereas it was observed to be 658.5 ± 211.1 L/m^2.h.bar for homeotropic films. This supports our hypothesis about the mass transfer properties of the films were significantly improved when the pores were along to permeation direction. Lastly, films exhibit $78.4\% \pm 3.4\%$ rejection of BSA for planar films whereas $37.5\% \pm 2.6\%$ rejection was observed in homeotropic films. Observation of these rejections during the filtration of the aqueous solutions of BSA, which clearly suggests that these films can potentially be developed as membranes for ultrafiltration purposes. (The data for the filtration of pure water, ethanol and BSA solution was represented in Appendix A.)

Table 4.1 Results of the filtrations tests performed using 80 μm-thick films synthesized from 20% RM257 and 80% 5CB, by weight.

Feed	Horizontal Pores		Orthogonal Pores	
	Permeance (L/m²·h·bar)	Rejection (%)	Permeance (L/m²·h·bar)	Rejection (%)
Pure Ethanol	24.7 ± 4.0	-	602.8 ± 178.1	-
Pure Water	1.6 ± 0.1	-	658.5 ± 211.1	-
1 g/L BSA in PBS	0.6 ± 0.1	78.4 ± 3.4	5.5 ± 2.0	37.5 ± 2.6
200 nm-in-diameter PS in water	2.4	ND (~100%)	4.5 ± 1.8	ND (~100%)

Overall, we characterized the microstructures of the films templated from liquid crystalline media. We found that pores of an average diameter of 10-40 nm with controlled directionality via LC director can be incorporated into the films, when constrained in a determined area. We showed that this area constraint can be succeeded either by covalently bonding the film to the supporting surfaces, determining the area by external surfaces (o-rings), or due to the inherent symmetry of the liquid crystalline phases (such as chiral liquid crystal phases). As a proof-of-concept study, we demonstrated that the films synthesized from the polymerization of the mixtures of reactive and non-reactive mesogens can potentially be used as ultrafiltration membranes. We showed that these films exhibit a consistent separation of the feed solutions and the permeances that depend on the direction of the pores. Here we note that we left the more detailed characterization of the ultrafiltration performance of the films to our future studies.

4.1.11. Direct Polymerization of Reactive Mesogen

Dense films were synthesized by polymerization of pure reactive mesogen (RM257). The alignment of the films were provided by the same procedure which was rubbing PVA coated surface for planar anchoring and using DMOAP coated glass slide for homeotropic anchoring. As seen in Figure 4.20, the alignments of the polymeric films were determined, successfully.
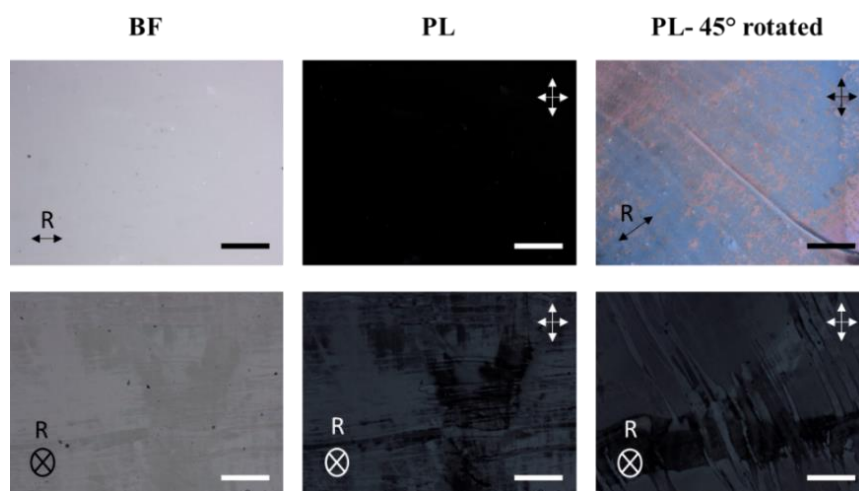
Figure 4.20 Bright field (left) and polarized (middle and right) light micrographs of the polymeric films (polymerized pure RM257) with planar (top row) and homeotropic (bottom row) anchoring. Scale bars: 50 μm

After the analysis of the alignment of the polymeric films via optical microscope, scanning electron microscopy was used to have an idea of the morphology of the polymers. As seen from Figure 4.21, porous structure was not observed in the micrographs of the polymeric films using SEM.
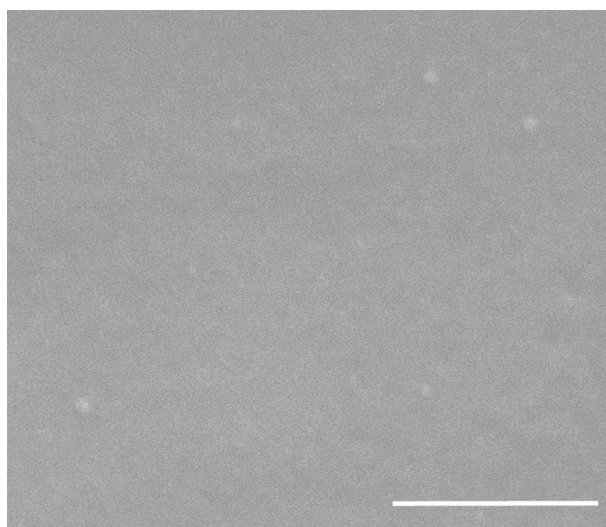
Figure 4.21 Scanning electron micrograph of the surface of the polymerized RM257 Scale bar: 500 nm

Then, in order to observe the effect of the direction of the polymer alignment on diffusion rate, the gas permeability tests of the films with planar and homeotropic anchoring were performed by using nitrogen and carbondioxide as feed. After the tests, we found that the flux in the case of the polymer with homeotropic anchoring was (nearly 5 times) faster than the polymer with planar anchoring. However, the values of the permeances were not consistent and when we compare the permeability of carbondioxide and nitrogen, we did not observe significant selectivity for these gases. (The results of the permeability tests were represented in Appendix B.)

4.2. Characterization of the Interaction of Particles in Liquid Crystalline Media

We used inorganic microparticles synthesized with different size and shapes. In this study, we chose cubic and leave shaped particles considering their anisotropic shapes. In addition to these, we preferred porous particles considering their wide application areas such as separations, catalysis, drug delivery, etc. For these purposes, we used zeolite 4A with truncated and sharp edges and ZIF-L as shown in Figure 4.22.
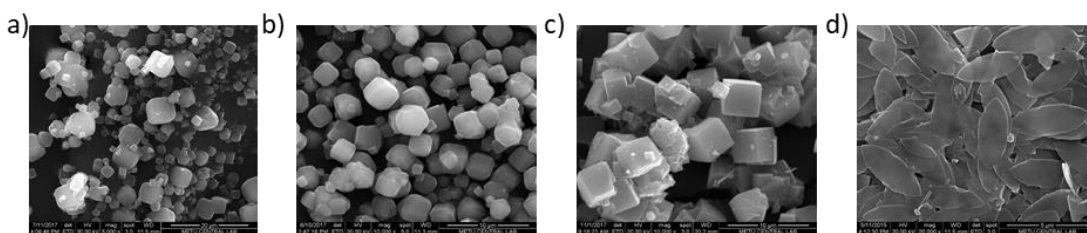
Figure 4.22 Scanning electron micrographs of zeolite 4A with (a) rounded edge truncated edge (left), sharp edge (middle) and ZIF-L (right)

4.2.1. Determination of Anchoring of LC on Microparticles' Surfaces

We first analyzed the anchoring of the LCs on the surfaces of these particles since the anchoring was not available in the literature and the anchoring condition on the surface of the particles is one of the important parameters affecting the alignment of the particles in liquid crystalline media (detailed in Chapter 2).

The analysis of the anchoring of the liquid crystal on the surface of the microparticles could be done by using polarized optical microscope in transmission mode since the liquid crystals have optical birefringence and the average orientation of LC molecules can be determined via transmitted light.[88]

We used zeolite 4A within sizes in the range of 2-6 µm. The particles were dispersed in LC media (5CB) and anchoring condition on the surface of the particles was analyzed by using optical microscope with cross polarizer and first order retardation plate (FOP). As seen in Figure 4.23, when the average alignment of the LCs was in the direction of one of the polarizers (shown as R, far from the particles), dark appearance was observed under polarized light. However, the distortion of the nematic director around the particles due to the anchoring condition at the surface of the particle resulted in a bright transmitted light as shown by white arrows in the polarized micrographs of Figure 4.23. Also, when FOP was inserted, red and blue colors were observed (shown by blue and red arrows in Figure 4.23). This coloring was consistent with the different alignment of LCs at two sides of the particles. Using this characterization, the LC anchoring on particle surface was determined as planar and a sketch of the ordering profile of the LCs at the vicinity of the particles was shown in

the right panel of Figure 4.23. (Here we note that we observed around 80% of the zeolite 4A particles exhibited planar anchoring of the LCs on their surfaces.)

Figure 4.23 Brightfield (BF), polarized light (PL) and first order retardation plate (FOP) micrographs of single, bare zeolite 4A dispersed in planar nematic cells. The sketch in the right panel shows the schematic representation of the LC director profile around the particle. Double headed arrow indicates the rubbing direction of the two glass slides. Scale bars: 5 μm.

In order to modify the LC anchoring at the surfaces of the particles, we functionalized the particle surfaces with dimethyloctadecyl[3-(trimethoxysilyl)propyl]ammonium chloride (DMOAP). With DMOAP functionalization, particles were expected to mediate homeotropic anchoring. We checked whether the particles mediate homeotropic anchoring using polarized light microscopy as shown from the images illustrated in Figure 4.24. The far field director in the images shown in Figure 4.24 is perpendicular to the imaging plane (inplane), so dark appearance was observed under polarized light. However, the distortion of the nematic director around the particles due to the anchoring condition at the surface of the particle resulted in a bright transmitted light as shown by white arrows in the polarized micrographs of Figure 4.22. Also, when FOP was inserted, red and blue colors were observed (shown by blue and red arrows in Figure 4.24). This coloring was consistent with the different alignment of LCs at two sides of the particles. We observed bright transmitted light at the four edges of the particle in a homeotropic cell, which suggests homeotropic anchoring of LCs at the surfaces of particles (which would appear dark if particle surface mediated planar anchoring). Using this characterization, the LC anchoring on particle surface was determined as homeotropic and a sketch of the ordering profile of the LCs at the vicinity of the particles was shown in the right panel of Figure 4.24. In

50

addition, when we compared the FOP micrographs of DMOAP coated particles and bare particles, it was seen that the red and blue colors around the particles were located at different sides and this situation pointed out the difference in the anchoring conditions on the surface of the particles. (Here we note that we observed around 90% of the zeolite 4A particles exhibited homeotropic anchoring of the LCs on their surfaces.)
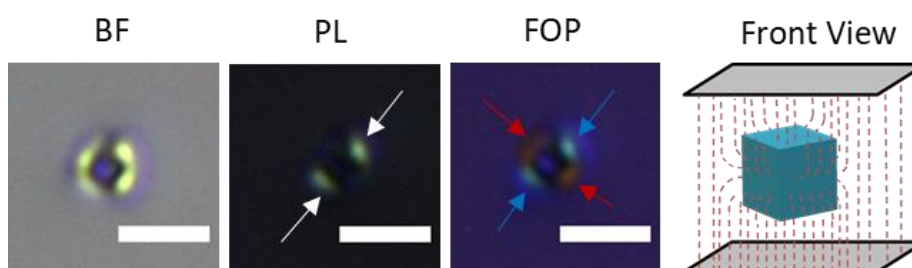
Figure 4.24 Brightfield (BF), polarized light (PL) and first order retardation plate (FOP) micrographs of single DMOAP coated zeolite 4A dispersed in homeotropic nematic cells and schematic representation of the LC director profile around the particle. Scale bars: 5 μm

In some cases, the anchoring condition around the particles may cause the formation of a defect structure around them. The examples of the common structures of defects we observed around zeolite 4A particles with rounded, truncated and sharp edges are shown in Figure 4.25. Defect structures around DMOAP coated particles with rounded edges were generally in the form of ring whereas S-shaped defects were formed around DMOAP coated, truncated particles (Figure 4.25). Beller and his collaborators evidenced that the structure of disclinations around the particles vary depending on the sharpness of the edges of the colloids by experimental and numerical methods.[93] The results of their studies showed that as the edges of the particles become sharper, disclinations start to wrap only the edges of the particles. Our observations were consistent with these predictions. As shown in Figure 4.25, as the sharpness of the particles varied, the shapes of the disclinations, which are indicated with solid red lines, changed and wrapped the edges of the particles.
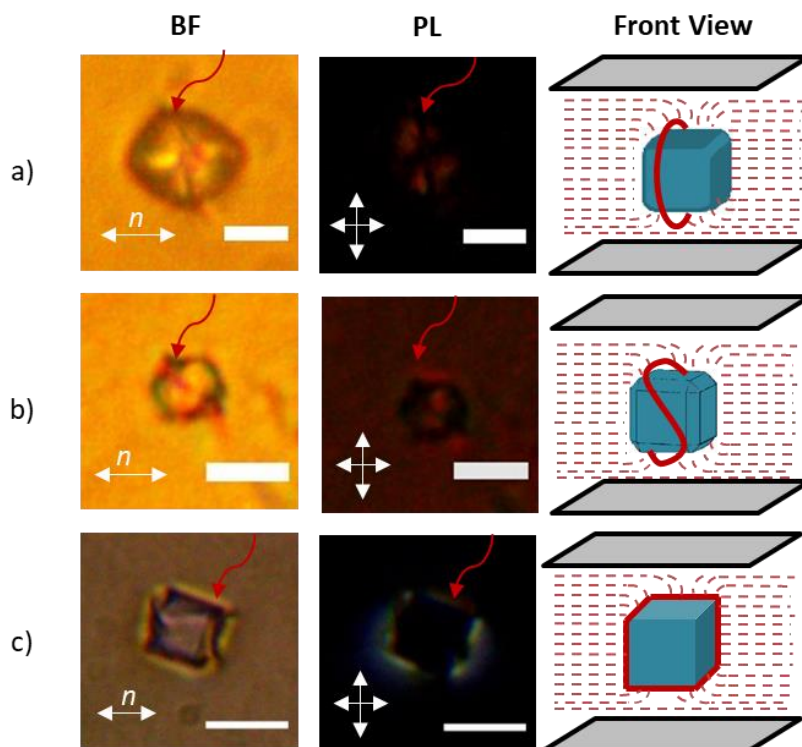
Figure 4.25 Brightfield (BF), polarized light (PL) micrographs of DMOAP coated zeolite 4A particles with (a) rounded, (b) truncated and (c) sharp edges and schematic representations of structure of defects around the particles in nematic planar cell. Red arrows in micrographs indicate the defects around the particles. Dashed and solid red lines in schematic illustration represent the alignment of the LCs and defects. Scale bars: 5µm

Next, we characterized the anchoring of LCs on the surfaces of ZIF-L particles. As seen in Figure 4.26, when the average alignment of the LCs was in the direction of one of the polarizers (shown as R, far from the particles), dark appearance was observed under polarized light. However, the distortion of the nematic director around the particles due to the anchoring condition at the surface of the particle resulted in a bright transmitted light as shown by white arrows in the polarized micrographs of Figure 4.26. At the end of this characterization, the LC anchoring on particle surface was determined as planar and a sketch of the ordering profile of the LCs at the vicinity of the particles was shown in the right panel of Figure 4.26. Here we note that we observed around 80% of the ZIF-L particles exhibited planar anchoring of the LCs on their surfaces.

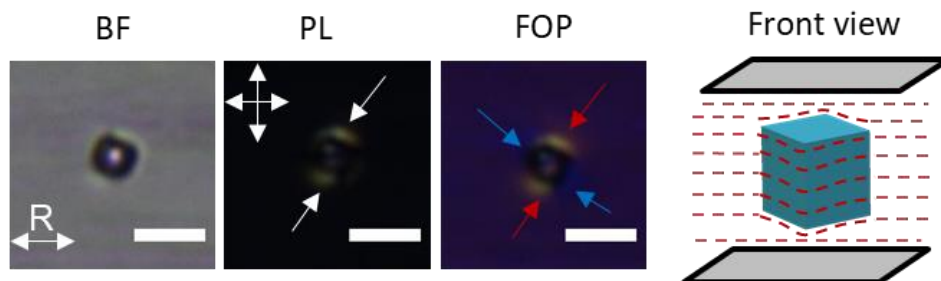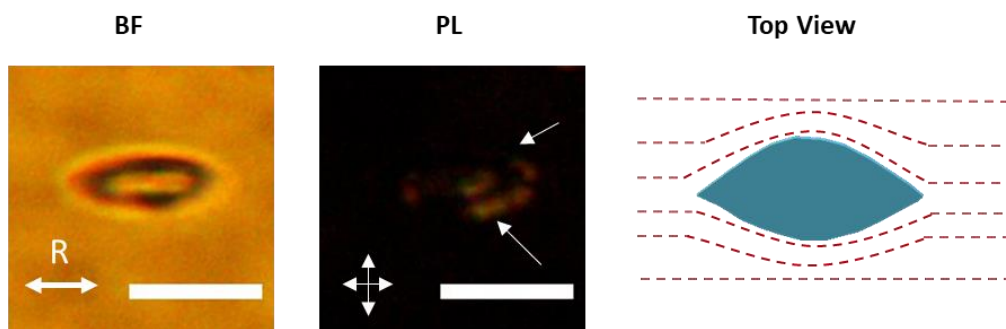Figure 4.26 Brightfield (BF), polarized light (PL) micrographs of single bare ZIF-L particle and schematic representation of the LC director profile around the particle dispersed in planar nematic cell. Scale bars: 10μm

We attempted to modify the surfaces of ZIF-L particles with DMOAP to mediate homeotropic anchoring of the LCs. However, we observed the ZIF-L particles to deform and maintain irregular shapes during the functionalization procedure.

4.2.2. Determination of Alignment of Zeolite 4A and ZIF-L Particles in Liquid Crystalline Media

After characterizing the surface anchoring of LCs on the surfaces of the zeolite 4A and ZIF-L particles, we next characterized the alignment of particles in LC media as a function of the surface anchoring, and shape of the particles.

For the analysis of the alignment of the particles in LC media, orientations of the single zeolite 4A and ZIF-L particles were examined by measuring the angles that the particles oriented in 5CB. In order to investigate the effect of the anchoring conditions on the orientations of the particles, we functionalized the surface of the zeolite 4A particles. When we analyzed bare zeolite 4A particles with sharp edges in planar and homeotropic cells, we evidenced that the particles maintain a position with an angle of 0° in planar medium whereas there was no significant tendency in the case of homeotropic cells as shown in Figure 4.27.
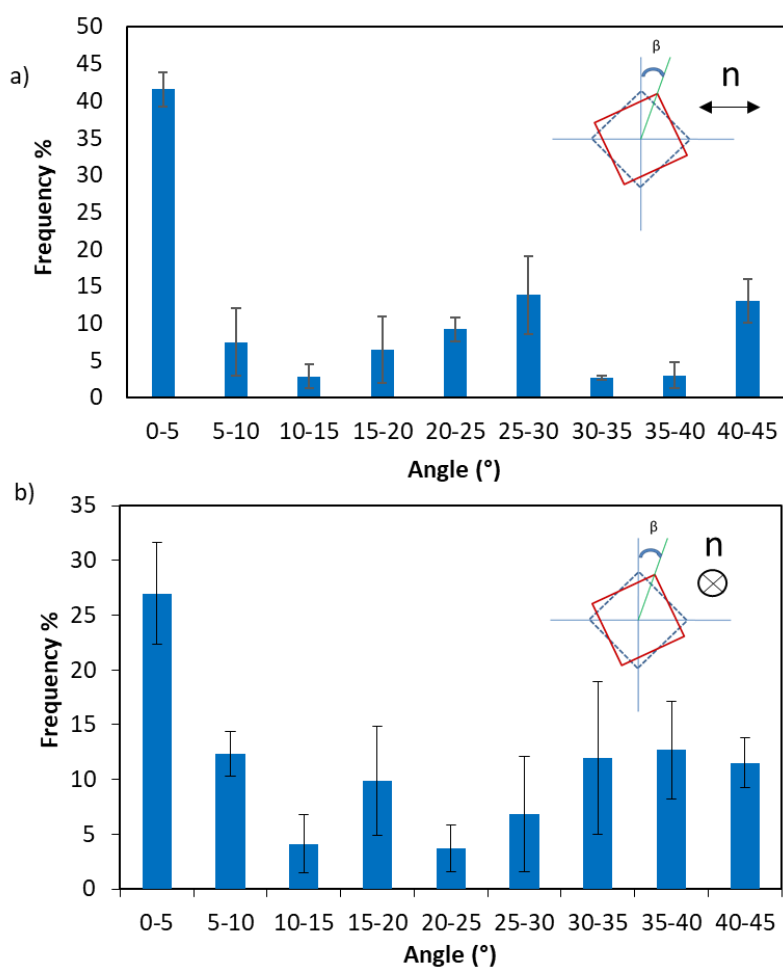
Figure 4.27 Angle distribution of the bare single zeolite 4A particles with sharp edges in a) planar cell b) homeotropic cell and schematic representation of orientations of the particles. β indicates the angle that the particle oriented in LC media.

When we functionalized the surface of the particle by coating with DMOAP, homeotropic anchoring on the surface of the particles was provided, so we repeated the analysis of the alignment of the particles with DMOAP coated zeolite 4A particles with sharp edges to observe the effect of anchoring condition on the orientation of the particles. As seen in Figure 4.28, DMOAP coated zeolite 4A particles had a tendency to stay with 0° and 45° when they were dispersed in planar cell. However, there was no specifically favoured orientation in the case of homeotropic anchoring and the reason of this behavior was thought as the effect of the disclinations around DMOAP coated particles in homeotropic cell.
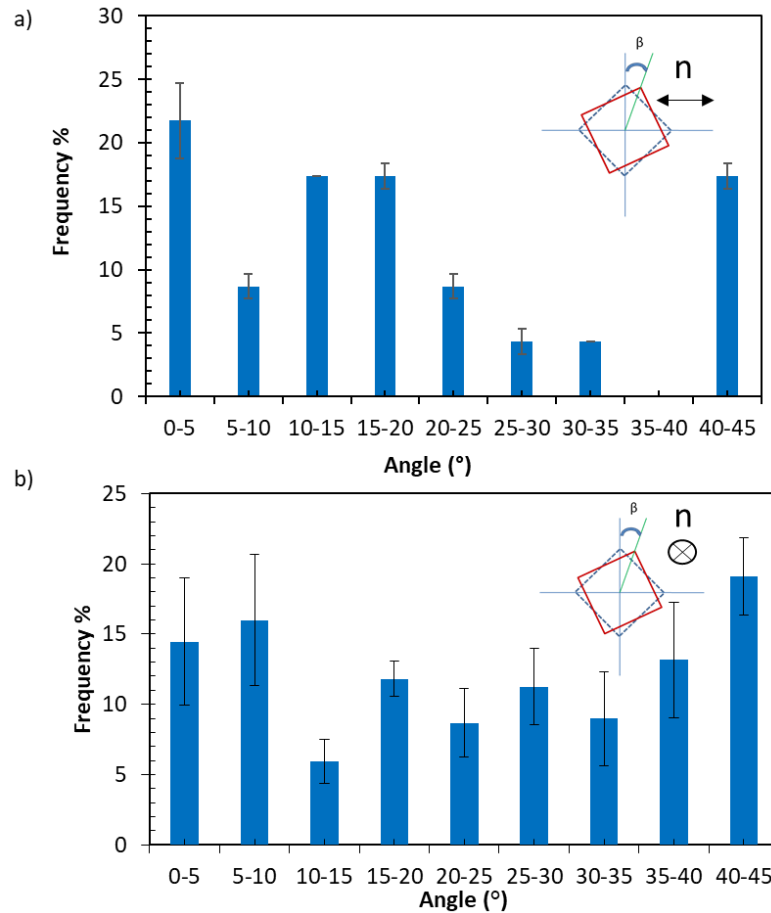
Figure 4.28 Angle distribution of DMOAP coated single zeolite 4A particles with sharp edges in a) planar cell b) homeotropic cell and schematic representation of orientations of the particles. β indicates the angle that the particle oriented in LC media.

Then, in order to investigate the effect of the sharpness of the particles to the orientation of the single particles in liquid crystalline media, zeolite 4A with rounded and truncated edges were also used for the analysis. When we analyzed the orientation of the single bare zeolite 4A with rounded edges (Figure 4.22a) and truncated edges (Figure 4.22b), we observed that the single particles dispersed in planar medium generally had a tendency to stay with an angle around 0° as shown in Figure 4.29a. On the other hand, DMOAP coated particles were oriented almost randomly in planar medium (Figure 4.29b). Therefore, we evidenced that although the structures of the defects formed around the single particles were varied with respect to the sharpness of the edges, it did not cause significant difference in the orientations of the single particles dispersed in LC media. The effects of the shape of the disclinations on the

orientation of the particles may be changed with respect to the size of the particles. However, we could not analyze the change in the effects of the shape of disclinations on the orientation with regard to size of the particles since the particles that we used were monodisperse.
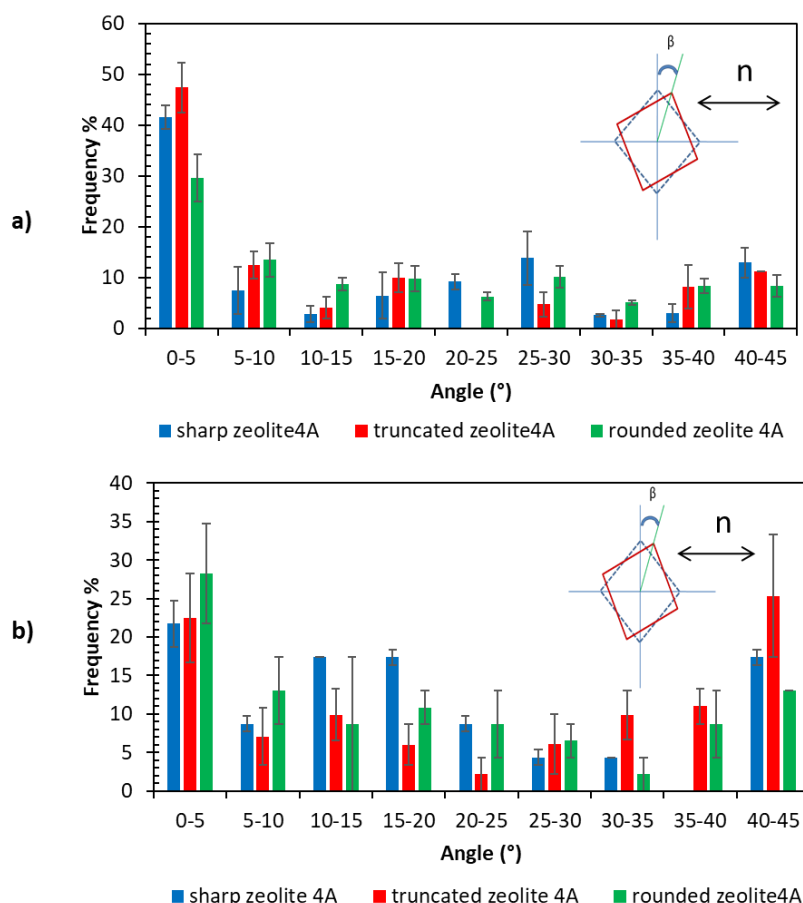
Figure 4.29 Angle distributions of (a) bare zeolite 4A with rounded, truncated and sharp edges and (b) DMOAP coated zeolite 4A with rounded, truncated and sharp edges. Schematic illustrations of the definition of the angles (β) represented on each histogram.

Then, in order to check whether the alignment of the particles was remained in the polymeric films, the analysis of the alignment of the zeolite 4A in polymeric films was done by using the particles with truncated edges. As a result, it was seen that the particles exhibited same behavior when they were dispersed in polymeric network. As

56

seen in Figure 4.30, single bare zeolite 4A with truncated edges had a tendency to stay with an angle of 0° in polymer in a similar manner of LC-media (Figure 4.29a.)
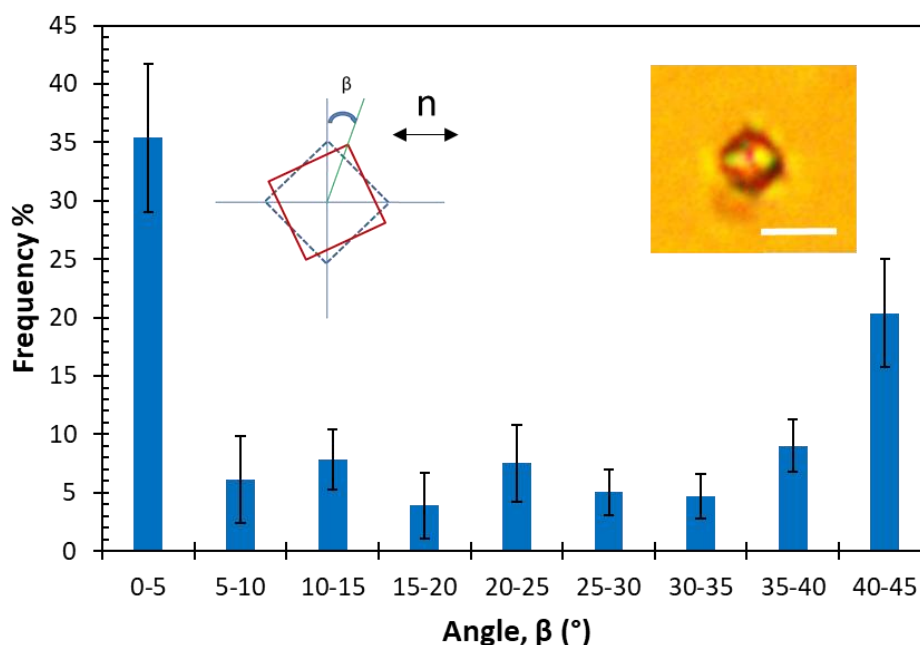
Figure 4.30 Angle distribution of single bare zeolite 4A with truncated edges in polymerized mixture of 20% wt monomer (RM257) and 80% wt LC (5CB) and brightfield (BF) micrograph of single bare zeolite 4A with truncated edges in polymeric network. Scale bar: 5μm

After the analysis of the orientation of the particles by using the optical microscope, we used scanning electron microscopy for imaging the alignment of the particles in polymeric network. When the cross section of the polymeric films containing the zeolite 4A particles with truncated edges was scanned (Figure 4.31), we saw that the orientation of the particles was compatible with the results of the analysis done by using the optical microscope .
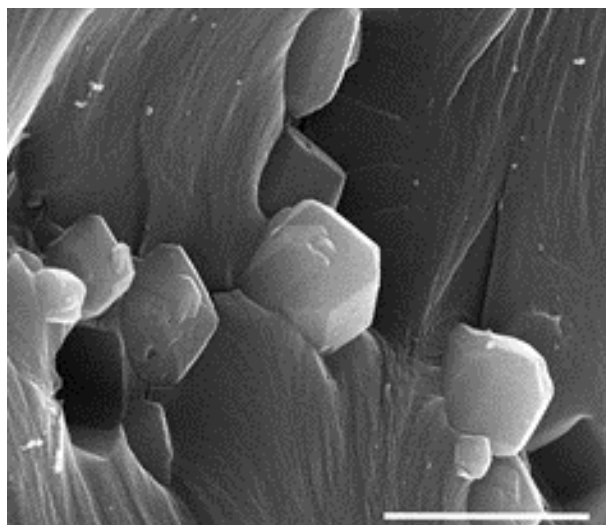
Figure 4.31 Scanning electron micrographs of cross section of polymerized mixture of 20% wt monomer (RM257) and 80% wt LC (5CB) containing zeolite 4A with truncated edges Scale bar: 5 μm

Next, we analyzed the alignment of bare single ZIF-L particles in LC media. As mentioned above, we did not functionalized the surface of the ZIF-L particles because of the deformations in the shape of particles, so we analyzed bare single ZIF-L particles dispersed in LC-media. As seen in Figure 4.32a, bare single ZIF-L particles had a tendency to stay with an angle of 0°. In order to calculate the rotation of the ZIF-L particles around x-axis, we used the change in the aspect ratio of the particles since we know the initial aspect ratio of monodisperse ZIF-L particles. As a result of this calculation, we found that the particles stayed with an angle of 80° around x axis as shown in Figure 4.32.
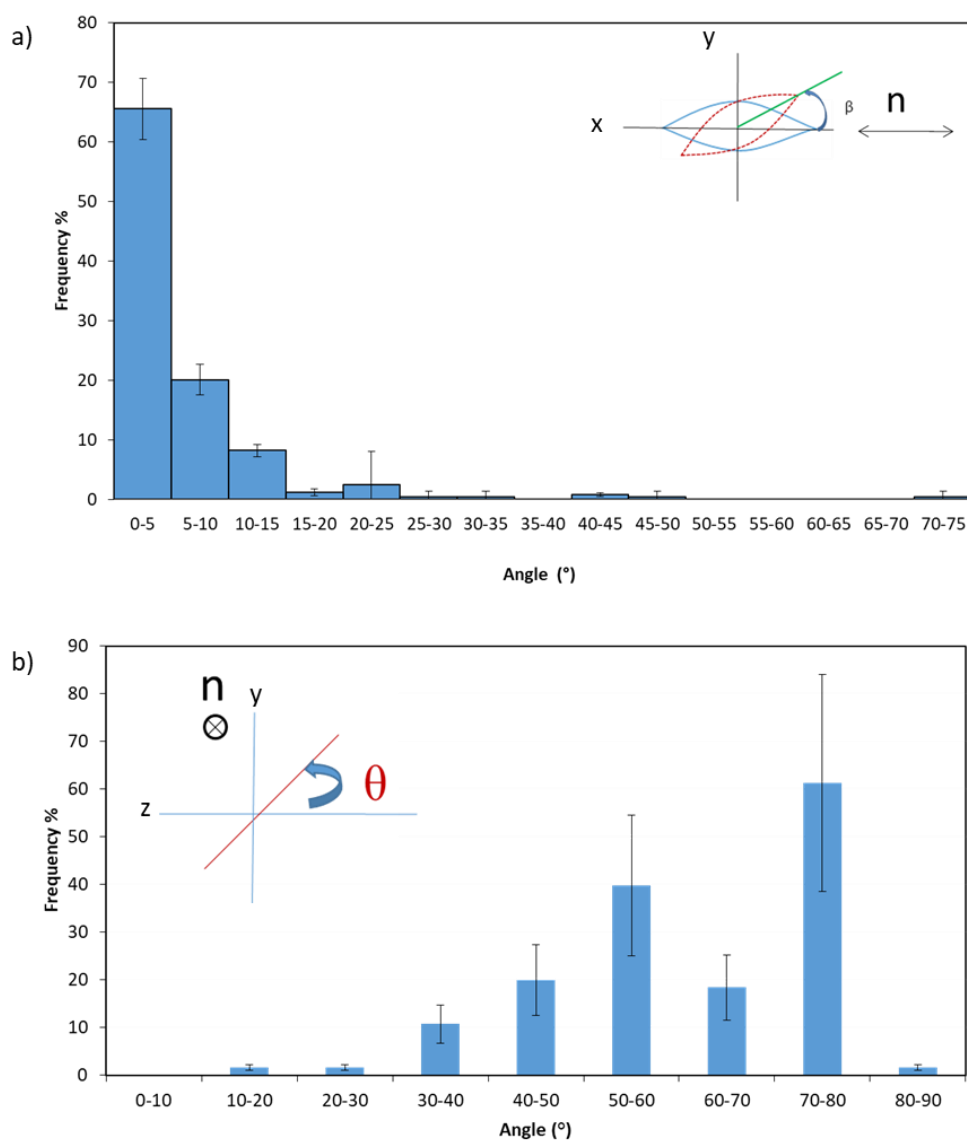
Figure 4.32 Angle distributions of isolated, bare ZIF-L particles in planar medium. (a) Rotation around z-axis, indicated by angle β and (b) rotation around x-axis, indicated by angle θ.

4.2.3. Analysis of the Assemblies of Zeolite 4A Particles in Liquid Crystalline Media

After the analysis of the orientations of the single particles in LC media, we investigated how the assemblies were formed by the multiple particles to determine whether the control over the form of the assemblies in the polymeric network is possible or not. In Figure 4.33, optical micrographs of the examples of the multiple

(double and triple) organizations of the particles were represented. As seen from Figure 4.33, the particles generally attached each other at the corners where the disclination rings located.
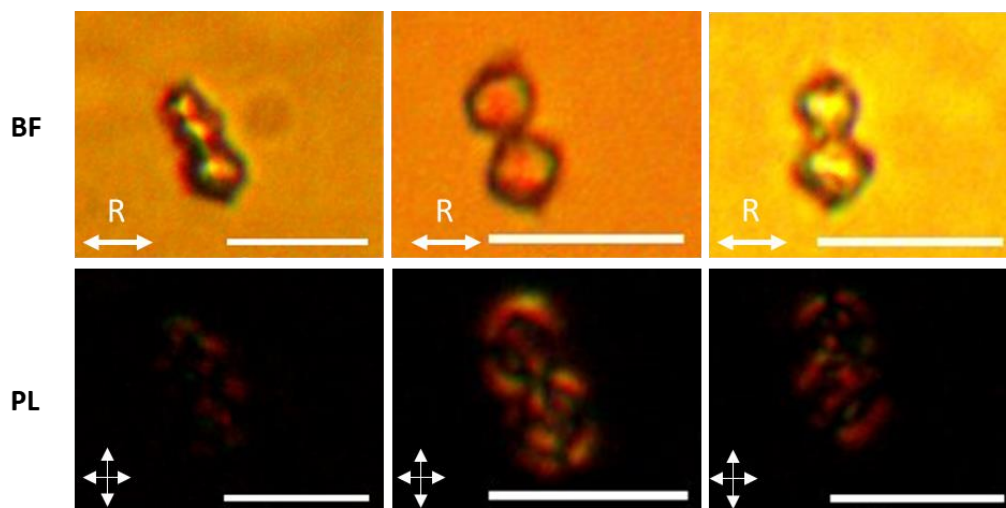
Figure 4.33 Brightfield (BF), polarized light (PL) micrographs of double and triple organizations of DMOAP coated zeolite 4A particles with truncated edges in polymerized mixture of 20% wt monomer (RM257) and 80% wt LC (5CB) in planar medium. Scale bars: 10µm

When we analyzed single DMOAP coated zeolite 4A particles with rounded edges in homeotropic medium, we observed that the defects with the shape of ring became more significant (Figure 4.34) than in planar medium (Figure 4.25a). In addition, the disclinations around the single particles were merged and became a larger ring around the assemblies as the particles formed multiple organizations and it causes aggregation as seen in Figure 4.34.
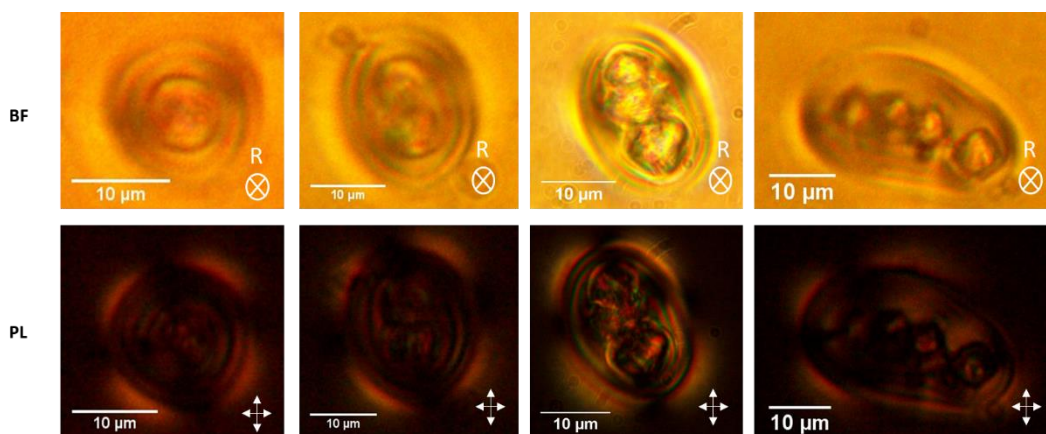
Figure 4.34 Brightfield (BF), polarized light (PL) micrographs of single DMOAP coated zeolite 4A particle with rounded edges and the multiple organizations they formed in LC-media.

CHAPTER 5

CONCLUSIONS

In this study, methods for the synthesis of porous polymeric films of area in the order of 1-10 cm^2 using liquid crystals as templates and determination of the alignment of the inorganic microparticles in LC media were provided. Firstly, we showed when photopolymerized films of reactive and non-reactive mesogen mixtures were constrained in an area during the extraction of the unreacted mesogens, open pores can be incorporated into the polymers. We characterized the morphologies of such films and found that the average diameter of the pores was in the range 10-40 nm, and can be tuned by varying the reactive monomer concentration. In addition, the method that we developed herein, provides control over the average direction of the pores through varying the nematic director, which suggest potential mass transfer advantages. Overall, the method presented in this study provides control over the pore size and directionality that would be difficult to achieve through the use of isotropic fluids. The methods that were developed in this study is generalizable. That is, the methods can also be applicable to other liquid crystalline phases such as cholesterics, blue phases, biaxial nematics etc., which would provide a rich palette of three-dimensional pore structures that would be advantageous in a scientific and technological perspective. The morphology of the films synthesized from liquid-crystal templates were also successfully demonstrated to be useful as an ultrafiltration membrane. A number of future directions could be suggested based on the findings in this study, some of which include characterization of the ultrafiltration performance of the membranes, functionalization of the pores (such as acidic or basic groups) and tuning the structure and geometry of the pores through the ordering symmetry of the liquid crystals. As the second part of this study, the self-assembly of the inorganic particles of different shapes incorporated into LCs were investigated. The cubic zeolite 4A particles in a size range of 2-6 μm with truncated, sharp or round edges were used. Also, leave shaped ZIF-L particles were used with 400 nm thickness and 1-4 and 5-10 μm in length

and width, respectively. We evidenced that the particles could be oriented in a preferred direction in both LC media and polymeric network. In addition, it was possible to form different three-dimensional defect structures by adjusting the anchoring conditions and sharpness of the particles. Determination and control over the symmetry of the defect structure is important since it provides control over the assemblies of nanoscopic species as shown in the literature.[94] Thus, the system that were analyzed in this study is open to future investigations of the assemblies of nanoscopic species such as nanoparticles and lipids at LC defects.

REFERENCES

(1) Leddy, H. A.; Haider, M. A.; Guilak, F. Diffusional Anisotropy in Collagenous Tissues: Fluorescence Imaging of Continuous Point Photobleaching. *Biophys. J.* **2006**, *91* (1), 311–316.

(2) Bukusoglu, E.; Bedolla Pantoja, M.; Mushenheim, P. C.; Wang, X.; Abbott, N. L. Design of Responsive and Active (Soft) Materials Using Liquid Crystals. *Annu. Rev. Chem. Biomol. Eng.* **2016**, *7* (1), 163–196.

(3) Wang, X.; Bukusoglu, E.; Miller, D. S.; Bedolla Pantoja, M. A.; Xiang, J.; Lavrentovich, O. D.; Abbott, N. L. Synthesis of Optically Complex, Porous, and Anisometric Polymeric Microparticles by Templating from Liquid Crystalline Droplets. *Adv. Funct. Mater.* **2016**, *26* (40), 7343–7351.

(4) Mondiot, F.; Wang, X.; De Pablo, J. J.; Abbott, N. L. Liquid Crystal-Based Emulsions for Synthesis of Spherical and Non-Spherical Particles with Chemical Patches. *J. Am. Chem. Soc.* **2013**, *135* (27), 9972–9975.

(5) Tamaoki, N. Cholesteric Liquid Crystals for Color Information Technology. *Adv. Mater.* **2001**, *13* (15), 1135–1147.

(6) Xie, P.; Zhang, R. Liquid Crystal Elastomers , Networks and Gels : Advanced Smart Materials. **2005**, 2529–2550.

(7) White, T. J.; Broer, D. J. Programmable and Adaptive Mechanics with Liquid Crystal Polymer Networks and Elastomers. *Nat. Mater.* **2015**, *14* (11), 1087–1098.

(8) De Haan, L. T.; Gimenez-Pinto, V.; Konya, A.; Nguyen, T. S.; Verjans, J. M. N.; Sánchez-Somolinos, C.; Selinger, J. V.; Selinger, R. L. B.; Broer, D. J.; Schenning, A. P. H. J. Accordion-like Actuators of Multiple 3D Patterned Liquid Crystal Polymer Films. *Adv. Funct. Mater.* **2014**, *24* (9), 1251–1258.

(9) De Haan, L. T.; Leclère, P.; Damman, P.; Schenning, A. P. H. J.; Debije, M. G. On-Demand Wrinkling Patterns in Thin Metal Films Generated from Self-Assembling Liquid Crystals. *Adv. Funct. Mater.* **2015**, *25* (9), 1360–1365.

(10)   Van Oosten, C. L.; Bastiaansen, C. W. M.; Broer, D. J. Printed Artificial Cilia from Liquid-Crystal Network Actuators Modularly Driven by Light. *Nat. Mater.* **2009**, *8* (8), 677–682.

(11)   Wei, R.; Zhou, L.; He, Y.; Wang, X.; Keller, P. Effect of Molecular Parameters on Thermomechanical Behavior of Side-on Nematic Liquid Crystal Elastomers. *Polymer (Guildf).* **2013**, *54* (20), 5321–5329.

(12)   Koenig, G. M.; De Pablo, J. J.; Abbott, N. L. Characterization of the Reversible Interaction of Pairs of Nanoparticles Dispersed in Nematic Liquid Crystals. *Langmuir* **2009**, *25* (23), 13318–13321.

(13)   Li, F.; Josephson, D. P.; Stein, A. Colloidal Assembly: The Road from Particles to Colloidal Molecules and Crystals. *Angew. Chemie - Int. Ed.* **2011**, *50* (2), 360–388.

(14)   Slowing, I. I.; Vivero-escoto, J. L.; Wu, C.; Lin, V. S. Mesoporous Silica Nanoparticles as Controlled Release Drug Delivery and Gene Transfection Carriers ☆. **2008**, *60*, 1278–1288.

(15)   Ghosh, P.; Han, G.; De, M.; Kim, C. K.; Rotello, V. M. Gold Nanoparticles in Delivery Applications ☆. **2008**, *60*, 1307–1315.

(16)   Agnihotri, S. A.; Mallikarjuna, N. N.; Aminabhavi, T. M. Recent Advances on Chitosan-Based Micro- and Nanoparticles in Drug Delivery B. **2004**, *100*, 5–28.

(17)   Castles, F.; Day, F. V.; Morris, S. M.; Ko, D. H.; Gardiner, D. J.; Qasim, M. M.; Nosheen, S.; Hands, P. J. W.; Choi, S. S.; Friend, R. H.; et al. Blue-Phase Templated Fabrication of Three-Dimensional Nanostructures for Photonic Applications. *Nat. Mater.* **2012**, *11* (7), 599–603.

(18)   Castles, F.; Morris, S. M.; Hung, J. M. C.; Qasim, M. M.; Wright, A. D.; Nosheen, S.; Choi, S. S.; Outram, B. I.; Elston, S. J.; Burgess, C.; et al. Stretchable Liquid-Crystal Blue-Phase Gels. *Nat. Mater.* **2014**, *13* (8), 817–821.

(19)   Ware, T. H.; McConney, M. E.; Wie, J. J.; Tondiglia, V. P.; White, T. J. Voxelated Liquid Crystal Elastomers. *Science (80-.).* **2015**, *347* (6225), 982–984.

(20)   White, T. J.; Serak, S. V.; Tabiryan, N. V.; Vaia, R. A.; Bunning, T. J. Polarization-Controlled, Photodriven Bending in Monodomain Liquid Crystal Elastomer Cantilevers. *J. Mater. Chem.* **2009**, *19* (8), 1080–1085.

(21)   Yu, Y.; Nakano, M.; Ikeda, T. Directed Bending of a Polymer Film by Light. *Nature* **2003**, *425* (6954), 145.

(22)   Sawa, Y.; Ye, F.; Urayama, K.; Takigawa, T.; Gimenez-Pinto, V.; Selinger, R. L. B.; Selinger, J. V. Shape Selection of Twist-Nematic-Elastomer Ribbons. *Proc. Natl. Acad. Sci.* **2011**, *108* (16), 6364–6368.

(23)   De Haan, L. T.; Sánchez-Somolinos, C.; Bastiaansen, C. M. W.; Schenning, A. P. H. J.; Broer, D. J. Engineering of Complex Order and the Macroscopic Deformation of Liquid Crystal Polymer Networks. *Angew. Chemie - Int. Ed.* **2012**, *51* (50), 12469–12472.

(24)   McConney, M. E.; Martinez, A.; Tondiglia, V. P.; Lee, K. M.; Langley, D.; Smalyukh, I. I.; White, T. J. Topography from Topology: Photoinduced Surface Features Generated in Liquid Crystal Polymer Networks. *Adv. Mater.* **2013**, *25* (41), 5880–5885.

(25)   Konya, A.; Gimenez-Pinto, V.; Selinger, R. L. B. Modeling Defects, Shape Evolution, and Programmed Auto-Origami in Liquid Crystal Elastomers. *Front. Mater.* **2016**, *3* (June), 1–7.

(26)   Kowalski, B. A.; Guin, T. C.; Auguste, A. D.; Godman, N. P.; White, T. J. Pixelated Polymers: Directed Self Assembly of Liquid Crystalline Polymer Networks. *ACS Macro Lett.* **2017**, *6* (4), 436–441.

(27)   Dai, M.; Picot, O. T.; Verjans, J. M. N.; De Haan, L. T.; Schenning, A. P. H. J.; Peijs, T.; Bastiaansen, C. W. M. Humidity-Responsive Bilayer Actuators Based on a Liquid-Crystalline Polymer Network. *ACS Appl. Mater. Interfaces* **2013**, *5* (11), 4945–4950.

(28) De Haan, L. T.; Verjans, J. M. N.; Broer, D. J.; Bastiaansen, C. W. M.; Schenning, A. P. H. J. Humidity-Responsive Liquid Crystalline Polymer Actuators with an Asymmetry in the Molecular Trigger That Bend, Fold, and Curl. *J. Am. Chem. Soc.* **2014**, *136* (30), 10585–10588.

(29) Pei, Z.; Yang, Y.; Chen, Q.; Terentjev, E. M.; Wei, Y.; Ji, Y. Mouldable Liquid-Crystalline Elastomer Actuators with Exchangeable Covalent Bonds. *Nat. Mater.* **2014**, *13* (1), 36–41.

(30) Feng, W.; Broer, D. J.; Liu, D. Oscillating Chiral-Nematic Fingerprints Wipe Away Dust. *Adv. Mater.* **2018**, *1704970*, 1704970.

(31) Gelebart, A. H.; Liu, D.; Mulder, D. J.; Leunissen, K. H. J.; van Gerven, J.; Schenning, A. P. H. J.; Broer, D. J. Photoresponsive Sponge-Like Coating for On-Demand Liquid Release. *Adv. Funct. Mater.* **2018**, *1705942*, 1705942.

(32) Iamsaard, S.; Aßhoff, S. J.; Matt, B.; Kudernac, T.; Cornelissen, J. J. L. M.; Fletcher, S. P.; Katsonis, N. Conversion of Light into Macroscopic Helical Motion. *Nat. Chem.* **2014**, *6* (3), 229–235.

(33) Eelkema, R.; Pollard, M. M.; Vicario, J.; Katsonis, N.; Ramon, B. S.; Bastiaansen, C. W. M.; Broer, D. J.; Feringa, B. L. Nanomotor Rotates Microscale Objects. *Nature* **2006**, *440* (7081), 163.

(34) Eelkema, R.; Pollard, M. M.; Katsonis, N.; Vicario, J.; Broer, D. J.; Feringa, B. L. Rotational Reorganization of Doped Cholesteric Liquid Crystalline Films. *J. Am. Chem. Soc.* **2006**, *128* (44), 14397–14407.

(35) Dierking, I. Polymer Network-Stabilized Liquid Crystals. *Adv. Mater.* **2000**, *12* (3), 167–181.

(36) Doane, J. W.; Golemme, A.; West, J. L.; Whitehead, J. B.; Wu, B.-G. Polymer Dispersed Liquid Crystals for Display Application. *Mol. Cryst. Liq. Cryst. Inc. Nonlinear Opt.* **1988**, *165* (1), 511–532.

(37) Kikuchi, H.; Yokota, M.; Hisakado, Y.; Yang, H.; Kajiyama, T. Polymer-Stabilized Liquid Crystal Blue Phases. *Nat. Mater.* **2002**, *1* (1), 64–68.

(38) Kempe, M. D.; Scruggs, N. R.; Verduzco, R.; Lal, J.; Kornfield, J. A. Self-Assembled Liquid-Crystalline Gels Designed from the Bottom up. *Nat. Mater.* **2004**, *3* (3), 177–182.

(39) Zhang, Y.; Zhou, L.; Yang, J.; Zhang, J.; Hai, M.; Zhang, L.; Li, F.; Zhang, C.; Yang, Z.; Yang, H.; et al. Effects of Crosslinking Agent/diluents/thiol on Morphology of the Polymer Matrix and Electro-Optical Properties of Polymer-Dispersed Liquid Crystal. *Liq. Cryst.* **2018**, *45* (5), 728–735.

(40) LeGrange, J. D.; Carter, S. A.; Fuentes, M.; Boo, J.; Freeny, A. E.; Cleveland, W.; Miller, T. M. Dependence of the Electro-Optical Properties of Polymer Dispersed Liquid Crystals on the Photopolymerization Process. *J. Appl. Phys.* **1997**, *81* (9), 59845991.

(41) Ohm, C.; Brehmer, M.; Zentel, R. Liquid Crystalline Elastomers as Actuators and Sensors. *Adv. Mater.* **2010**, *22* (31), 3366–3387.

(42) Boothby, J. M.; Ware, T. H. Dual-Responsive, Shape-Switching Bilayers Enabled by Liquid Crystal Elastomers. *Soft Matter* **2017**, *13*, 4349–4356.

(43) Hogan, P. M.; Tajbakhsh, A. R.; Terentjev, E. M. Uv Manipulation of Order and Macroscopic Shape in Nematic Elastomers. *Phys. Rev. E - Stat. Physics, Plasmas, Fluids, Relat. Interdiscip. Top.* **2002**, *65* (4), 10.

(44) Thomsen, D. L.; Keller, P.; Naciri, J.; Pink, R.; Jeon, H.; Shenoy, D.; Ratna, B. R. Liquid Crystal Elastomers with Mechanical Properties of a Muscle. *Macromolecules* **2001**, *34* (17), 5868–5875.

(45) Ohm, C.; Serra, C.; Zentel, R. A Continuous Flow Synthesis of Micrometer-Sized Actuators from Liquid Crystalline Elastomers. *Adv. Mater.* **2009**, *21* (47), 4859–4862.

(46) De Haan, L. T.; Schenning, A. P. H. J.; Broer, D. J. Programmed Morphing of Liquid Crystal Networks. *Polym. (United Kingdom)* **2014**, *55* (23), 5885–5896.

(47) Tajbakhsh, A. R.; Terentjev, E. M. Spontaneous Thermal Expansion of Nematic Elastomers. *Eur. Phys. J. E* **2001**, *6* (2), 181–188.

(48) Ellahi, M.; Liu, F.; Song, P.; Gao, Y.; Rafique, M. Y.; Khan, D. F.; Cao, H.; Yang, H. Characterization and Morphology of Polymer-Dispersed Liquid Crystal Films. *Soft Mater.* **2014**, *12* (3), 339–345.

(49) He, J.; Yan, B.; Yu, B.; Wang, S.; Zeng, Y.; Wang, Y. The Effect of Molecular Weight of Polymer Matrix on Properties of Polymer-Dispersed Liquid Crystals. *Eur. Polym. J.* **2007**, *43* (6), 2745–2749.

(50) Ellahi, M.; Liu, F.; Song, P.; Gao, Y.; Cao, H.; Rafique, M. Y.; Khaskheli, M. A.; Zubair Iqbal, M.; Yang, H. Influence of the Multi-Functional Epoxy Monomers Structure on the Electro-Optical Properties and Morphology of Polymer-Dispersed Liquid Crystal Films. *Polym. Bull.* **2013**, *70* (11), 2967–2980.

(51) Wei, Y.; Jang, C. H. Liquid Crystal as Sensing Platforms for Determining the Effect of Graphene Oxide-Based Materials on Phospholipid Membranes and Monitoring Antibacterial Activity. *Sensors Actuators, B Chem.* **2018**, *254*, 72–80.

(52) Heo, I. S.; Park, S. Y. Smart Shell Membrane Prepared by Microfluidics with Reactive Nematic Liquid Crystal Mixture. *Sensors Actuators, B Chem.* **2017**, *251*, 658–666.

(53) Hunter, J. T.; Abbott, N. L. Dynamics of the Chemo-Optical Response of Supported Films of Nematic Liquid Crystals. *Sensors Actuators, B Chem.* **2013**, *183*, 71–80.

(54) Marshall, J. E.; Gallagher, S.; Terentjev, E. M.; Smoukov, S. K. Anisotropic Colloidal Micromuscles from Liquid Crystal Elastomers. *J. Am. Chem. Soc.* **2014**, *136* (1), 474–479.

(55) Boothby, J. M.; Ware, T. H. Dual-Responsive, Shape-Switching Bilayers Enabled by Liquid Crystal Elastomers. *Soft Matter* **2017**.

(56) Schenning, A. P. H. J.; Gonzalez-Lemus, Y. C.; Shishmanova, I. K.; Broer, D. J. Nanoporous Membranes Based on Liquid Crystalline Polymers. *Liq. Cryst.* **2011**, *38* (11–12), 1627–1639.

(57)   Broer, D. J.; Mol, G. N.; Van Haaren, J. A. M. M.; Lub, J. Photo-Induced Diffusion in Polymerizing Chiral-Nematic Media. *Adv. Mater.* **1999**, *11* (7), 573–578.

(58)   Gin, D. L.; Bara, J. E.; Noble, R. D.; Elliott, B. J. Polymerized Lyotropic Liquid Crystal Assemblies for Membrane Applications. *Macromol. Rapid Commun.* **2008**, *29* (5), 367–389.

(59)   Gin, D. L.; Gray, D. H.; Smith, R. C.; Uni-, W. M. R. Polymerizable Liquid Crystals as Building Blocks for Functional , Nanostructured Materials. **1999**, No. 10, 1509–1522.

(60)   Bara, J. E.; Kaminski, A. K.; Noble, R. D.; Gin, D. L. Influence of Nanostructure on Light Gas Separations in Cross-Linked Lyotropic Liquid Crystal Membranes. *J. Memb. Sci.* **2007**, *288* (1–2), 13–19.

(61)   Feng, P.; Bu, X.; Stucky, G. D.; Pine, D. J. Monolithic Mesoporous Silica Templated by Microemulsion Liquid Crystals [23]. *J. Am. Chem. Soc.* **2000**, *122* (5), 994–995.

(62)   Zhou, M.; Kidd, T. J.; Noble, R. D.; Gin, D. L. Supported Lyotropic Liquid-Crystal Polymer Membranes: Promising Materials for Molecular-Size-Selective Aqueous Nanofiltration. *Adv. Mater.* **2005**, *17* (15), 1850–1853.

(63)   Wang, X.; Bukusoglu, E.; Abbott, N. L. A Practical Guide to the Preparation of Liquid Crystal-Templated Microparticles. *Chem. Mater.* **2017**, *29* (1), 53–61.

(64)   Wang, J.; Eijkel, J. C. T.; Jin, M.; Xie, S.; Yuan, D.; Zhou, G.; van den Berg, A.; Shui, L. Microfluidic Fabrication of Responsive Hierarchical Microscale Particles from Macroscale Materials and Nanoscale Particles. *Sensors Actuators, B Chem.* **2017**, *247*, 78–91.

(65)   Sadati, M.; Zhou, Y.; Melchert, D.; Guo, A.; Martínez-González, J. A.; Roberts, T. F.; Zhang, R.; de Pablo, J. J. Spherical Nematic Shell with Prolate Ellipsoidal Core. *Soft Matter* **2017**, *13* (41).

(66)   Miller, D. S.; Wang, X.; Abbott, N. L. Design of Functional Materials Based on Liquid Crystalline Droplets. *Chem. Mater.* **2014**, *26* (1), 496–506.

(67) Tin, P. S.; Chung, T. S.; Liu, Y.; Wang, R.; Liu, S. L.; Pramoda, K. P. Effects of Cross-Linking Modification on Gas Separation Performance of Matrimid Membranes. *J. Memb. Sci.* **2003**, *225* (1–2), 77–90.

(68) Bos, A.; Pünt, I.; Strathmann, H.; Wessling, M. Suppression of Gas Separation Membrane Plasticization by Homogeneous Polymer Blending. *AIChE J.* **2001**, *47* (5), 1088–1093.

(69) Chung, T. S.; Shao, L.; Tin, P. S. Surface Modification of Polyimide Membranes by Diamines for H2 and CO2 Separation. *Macromol. Rapid Commun.* **2006**, *27* (13), 998–1003.

(70) Paul, D. R.; Kemp, D. R. Containing Adsorptive Fillers. *J. Polym. Sci. Polym. Symp.* **1973**, *93* (41), 79–93.

(71) Ravnik, M.; Mus, I. Two-Dimensional Nematic Colloidal Crystals Self-Assembled by Topological Defects. *Science (80-.).* **2006**, *313* (August), 954–958.

(72) Poulin, P.; Weitz, D. a. Inverted and Multiple Nematic Emulsions. *Phys. Rev. E* **1998**, *57* (1), 626–637.

(73) Loudet, J. C.; Barois, P.; Poulin, P. Colloidal Ordering from Phase Separation in a Liquid-Crystalline Continuous Phase. *Nature* **2000**, *407* (6804), 611–613.

(74) Lapointe, C. P.; Mason, T. G.; Smalyukh, I. I. Shape-Controlled Colloidal Interactions in Nematic Liquid Crystals. *Science (80-.).* **2009**, *326* (5956), 1083–1086.

(75) Hung, F. R.; Bale, S. Faceted Nanoparticles in a Nematic Liquid Crystal: Defect Structures and Potentials of Mean Force. *Mol. Simul.* **2009**, *35* (10–11), 822–834.

(76) Yan, Y.; Davis, M. E.; Gavalas, G. R. Preparation of Zeolite ZSM-5 Membranes by In-Situ Crystallization on Porous α-Al2O3. *Ind. Eng. Chem. Res.* **1995**, *34* (5), 1652–1661.

(77) Yang, X.; Albrecht, D.; Caro, J. Revision of Charnell's Procedure towards the Synthesis of Large and Uniform Crystals of Zeolites A and X. *Microporous Mesoporous Mater.* **2006**, *90* (1–3 SPEC. ISS.), 53–61.

(78) Mohamed, R. M.; Fouad, O. A.; Ismail, A. A.; Ibrahim, I. A. Influence of Crystallization Times on the Synthesis of Nanosized ZSM-5. *Mater. Lett.* **2005**, *59* (27), 3441–3444.

(79) Bux, H.; Chmelik, C.; Krishna, R.; Caro, J. Ethene/ethane Separation by the MOF Membrane ZIF-8: Molecular Correlation of Permeation, Adsorption, Diffusion. *J. Memb. Sci.* **2011**, *369* (1–2), 284–289.

(80) Chen, R.; Yao, J.; Gu, Q.; Smeets, S.; Baerlocher, C.; Gu, H.; Zhu, D.; Morris, W.; Yaghi, O. M.; Wang, H. A Two-Dimensional Zeolitic Imidazolate Framework with a Cushion-Shaped Cavity for CO2adsorption. *Chem. Commun.* **2013**, *49* (82), 9500–9502.

(81) Vinh-Thang, H.; Kaliaguine, S. Predictive Models for Mixed-Matrix Membrane Performance: A Review. *Chem. Rev.* **2013**, *113* (7), 4980–5028.

(82) Bernardo, P.; Drioli, E.; Golemme, G. Membrane Gas Separation : A Review / State of the Art. **2009**, 4638–4663.

(83) Adewole, J. K.; Ahmad, A. L.; Ismail, S.; Leo, C. P. Current Challenges in Membrane Separation of CO2 from Natural Gas: A Review. *Int. J. Greenh. Gas Control* **2013**, *17*, 46–65.

(84) Şen, D.; Kalipçilar, H.; Yilmaz, L. Development of Polycarbonate Based Zeolite 4A Filled Mixed Matrix Gas Separation Membranes. *J. Memb. Sci.* **2007**, *303* (1–2), 194–203.

(85) Oral, E. E.; Yilmaz, L.; Kalipcilar, H. Effect of Gas Permeation Temperature and Annealing Procedure on the Performance of Binary and Ternary Mixed Matrix Membranes of Polyethersulfone, SAPO-34, and 2-Hydroxy 5-Methyl Aniline. *J. Appl. Polym. Sci.* **2014**, *131* (17), 8498–8505.

(86) Prathap Chandran, S.; Mondiot, F.; Mondain-Monval, O.; Loudet, J. C. Photonic Control of Surface Anchoring on Solid Colloids Dispersed in Liquid Crystals. *Langmuir* **2011**, *27* (24), 15185–15198.

(87) Smaïhi, M.; Gavilan, E.; Durand, J. O.; Valtchev, V. P. Colloidal Functionalized Calcined Zeolite Nanocrystals. *J. Mater. Chem.* **2004**, *14* (8), 1347–1351.

(88) Miller, D. S.; Carlton, R. J.; Mushenheim, P. C.; Abbott, N. L. Introduction to Optical Methods for Characterizing Liquid Crystals at Interfaces. *Langmuir* **2013**, *29* (10), 3154–3169.

(89) Kamarudin, M. A.; Khan, A. A.; Williams, C.; Rughoobur, G.; Said, S. M.; Nosheen, S.; Flewitt, A. J.; Qasim, M. M.; Wilkinson, T. D. Self-Assembled Liquid Crystalline Nanotemplates and Their Incorporation in Dye-Sensitised Solar Cells. *Electrochim. Acta* **2016**, *222*, 657–667.

(90) Discher, D. E.; Janmey, P.; Wang, Y. L. Tissue Cells Feel and Respond to the Stiffness of Their Substrate. *Science* **2005**, *310* (5751), 1139–1143.

(91) Chang, C. K.; Bastiaansen, C. M. W.; Broer, D. J.; Kuo, H. L. Alcohol-Responsive, Hydrogen-Bonded, Cholesteric Liquid-Crystal Networks. *Adv. Funct. Mater.* **2012**, *22* (13), 2855–2859.

(92) Chang, C. K.; Bastiaansen, C. W. M.; Broer, D. J.; Kuo, H. L. Discrimination of Alcohol Molecules Using Hydrogen-Bridged Cholesteric Polymer Networks. *Macromolecules* **2012**, *45* (11), 4550–4555.

(93) Beller, D. A.; Gharbi, M. A.; Liu, I. B. Shape-Controlled Orientation and Assembly of Colloids with Sharp Edges in Nematic Liquid Crystals. *Soft Matter* **2015**, *11* (6), 1078–1086.

(94) Wang, X.; Miller, D. S.; Bukusoglu, E.; Pablo, J. J. De; Abbott, N. L. Topological Defects in Liquid Crystals as Templates for Molecular Self-Assembly. *Nat. Mater.* **2015**, *15* (September), 1–9.
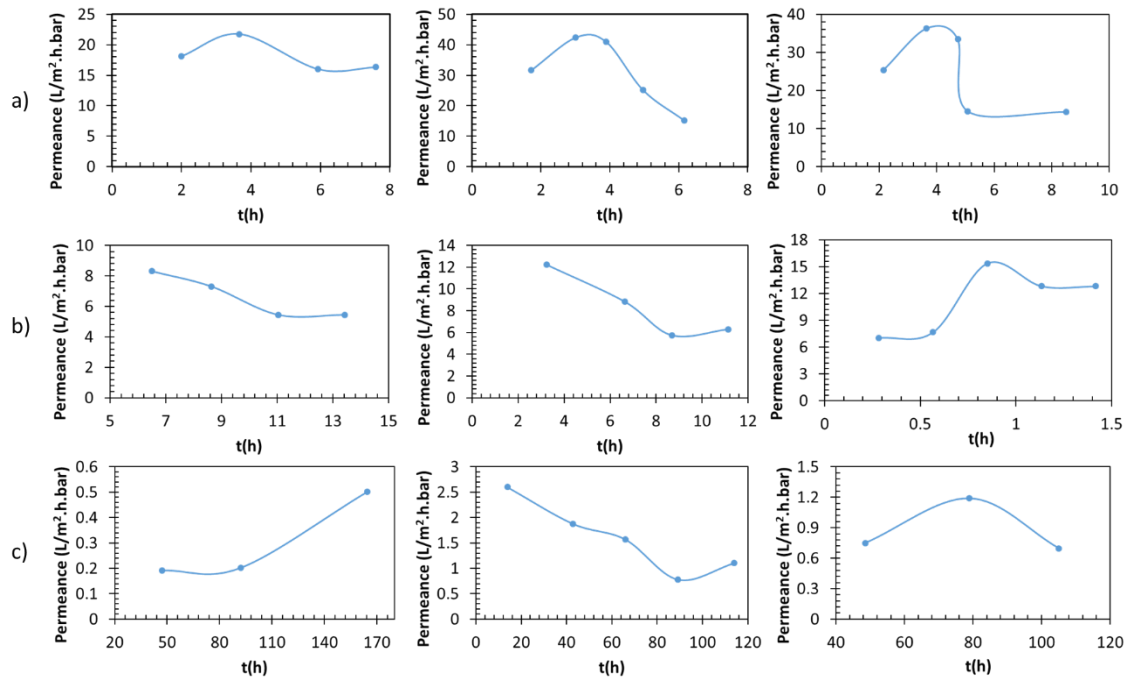
APPENDIX A

FILTRATION RESULTS

Figure A.1 The permeance results of the filtration of (a) ethanol, (b) pure water and (c) BSA solution (1 g/L BSA in PBS) in the case of membrane with horizontal pores
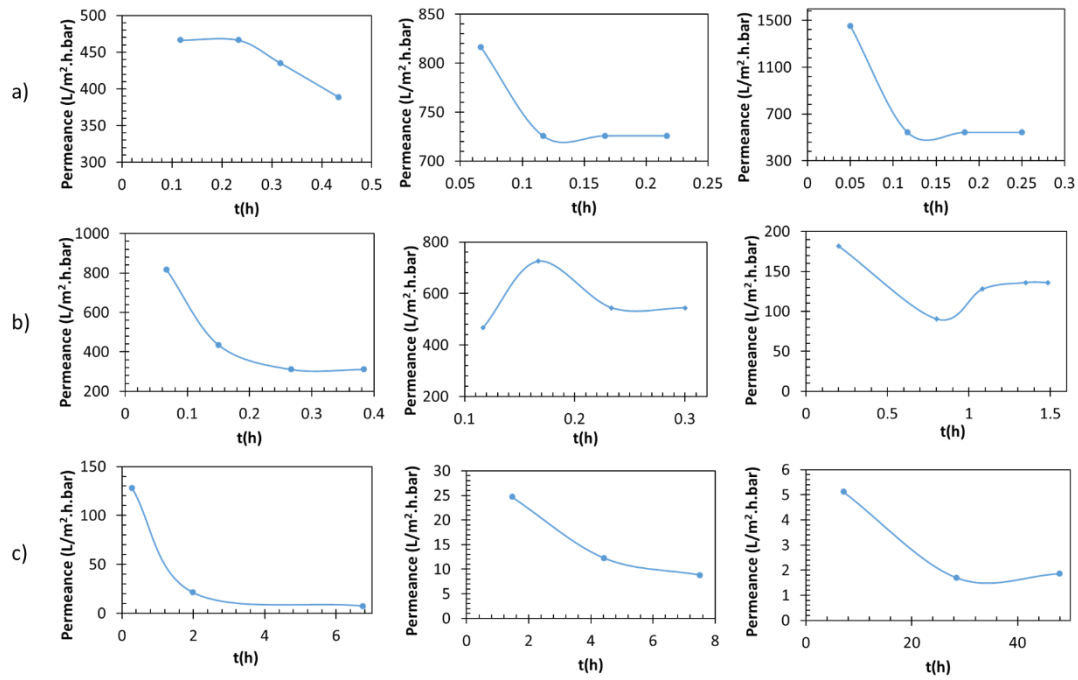
Figure A.2 The permeance results of the filtration of (a) ethanol, (b) pure water and (c) BSA solution (1 g/L BSA in PBS) in the case of membrane with orthogonal pores

APPENDIX B

RESULTS OF GAS PERMEATION TESTS

Table B.1. The results of gas permeability tests of planar and homeotropic polymeric films with a thickness of 40 μm

	Planar			Homeotropic	
	N_2 (barrer)	CO_2 (barrer)		N_2 (barrer)	CO_2 (barrer)
M1	34	32	**M1**	166	214
M2	3266	6061	**M2**	27355	27099
M3	4242	3025	**M3**	23743	31621